Study of Optical and Electrical Properties of Plasma Polymerized 1,2-Diaminocyclohexane Thin Films Synthesized by AC and RF Power Source

by

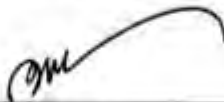Md. Mahmud Hasan

MASTER OF PHILOSOPHY IN PHYSICS

Department of Physics

BANGLADESH UNIVERSITY OF ENGINEERING AND TECHNOLOGY

June 2021

The thesis titled "Study of Optical and Electrical Properties of Plasma Polymerized 1,2-Diaminocyclohexane Thin Films Synthesized by AC and RF Power Source" submitted by Md. Mahmud Hasan, Roll No.: 0416143006F, Session: April-2016, has been accepted as satisfactory in partial fulfilment of the requirement for the degree MASTER OF PHILOSOPHY IN PHYSICS on 12 June, 2021.

BOARD OF EXAMINERS

1. Dr. Mohammad Jellur Rahman (Supervisor)
Associate Professor
Department of Physics, BUET, Dhaka.
        Chairman

2. Dr. Md. Rafi Uddin
Professor and Head
Department of Physics, BUET, Dhaka.
        Member
(Ex-officio)

3. Dr. Mohammed Abdul Basith
Professor
Department of Physics, BUET, Dhaka.
        Member

4. Dr. Muhammad Rakibul Islam
Associate Professor
Department of Physics, BUET, Dhaka.
        Member

5. Dr. Md. Abu Hashan Bhuiyan
Former Professor, Dept. of Physics, BUET
48/5-A, Tower Building
BUET R/A, Dhakeshwari Campus
BUET, Dhaka.
        Member
(External)

Candidate's Declaration

It is hereby declared that this thesis or any part of it has not been submitted elsewhere for the award of any degree or diploma.

Md. Mahmud Hasan

DEDICATED

TO

MY BELOVED PARENTS

Acknowledgements

Abstract

Smooth, transparent plasma polymerized (1,2-diaminocyclohexane) (PPDACH) thin films have been prepared on to glass substrates under AC (50 Hz) and RF (13.56 MHz) plasma using a capacitively coupled reactor. RF plasma deposited PPDACH thin films are observed smoother compared to AC plasma deposited thin films, which is confirmed from the atomic force microscopy images. However, mosaic-like structure is observed in the AC plasma deposited films, which are thermally more stable (up to ~280 ^{o}C) compared to RF deposited thin films. The at% of C and N in the thin films increases with increasing film thickness. Appearance of new absorption peaks in the FTIR spectra confirms structural changes in the plasma polymer owing to the degradation or re-organization of the monomer molecules during the plasma polymerization. The direct band gap values of the PPDACH (AC) thin films increase from 3.02 to 3.15 eV with the increase of film thickness, while nearly equal (~ 4.04 eV) for the RF PPDACH thin films. Schottky type electrical conduction mechanism is observed to be dominant in the PPDACH (AC) thin films, whereas space charge limited conduction is operative in the PPDACH (RF) thin films. Other optical parameters such as refractive index, extinction coefficient, Urbach energy, steepness parameter are also calculated to understand their applicability in different electronic and optoelectronic devices like optical coating, photovoltaic cells, etc.

CONTENTS

List of Figures

List of Tables

List of Abbreviations

AC	Alternating Current
DC	Direct Current
λ	Wavelength
Al	Aluminum
RF	Radio Frequency
DTA	Differential Thermal Analysis
DTG	Differential Thermograph
FTIR	Fourier Transform Infrared
FESEM	Field Emission Scanning Electron Microscopy
EDX	Energy dispersive X-ray
UV-vis	Ultraviolet-Visible
k_B	Boltzmann constant
K	Extinction coefficient
PECVD	Plasma Enhanced Chemical Vapor Deposition
A	Absorbance
T	Transmittance
α	Absorption coefficient
$E_{g(d)}$	Direct Band Gap
$E_{g(i)}$	Indirect Band Gap
E_u	Urbach Energy
σ_s	Steepness Parameter
μ	Refractive index
n	Power index
ε_0	Permittivity of Free Space
J	Current density
ΔE	Activation Energy
ν	Frequency
h	Planck constant
d	Thickness

CHAPTER 1
INTRODUCTION

1.1 Introduction

A thin film is a very thin layer of material ranging from fractions of a nanometer to several micrometers in thickness. Scientifically, a thin film is a two dimensional thin layer of material formed atom by atom or molecule by molecule. The earliest use of thin films is as protective coating. A new branch of physics called 'thin film technology' is being produced by remarkable growth of thin film development in the field of optoelectronic devices, manufacturing technologies, new materials development, etc. through research. Over the past few decades, thin-film technology has made tremendous progress due to the industrial requirement for effective thin-film microelectronic products. Recently, organic thin films have gained much attention to the researchers because organic semiconductor based device technology is relatively economical and easy to fabricate compared with the inorganic devices.

Plasma polymerization is an important technique to fabricate thin polymer films from a variety of organic and organometallic starting materials. The plasma polymerization technique involves DC, AC, RF, pulsed and magnetron assisted plasmas. Due to the light weight and their intriguing physical and chemical properties, polymer thin films have shown a number of applications in modern science and technology. The materials obtained by plasma polymerization are significantly different from conventional polymers and also different from most inorganic materials. In the last few decades, glow discharge plasma enhanced chemical vapor deposition (PECVD) has been popularly used to deposit thin films and recognized as a versatile technique among other various deposition methods such as chemical method [1], vacuum evaporation method [2], Successive Ionic Layer Adsorption and Reaction (SILAR) method [3], autocatalytic method [4] etc. Thin films with certain bulk properties needed for a specific application that can be prepared on various substrates from almost any organic vapor by plasma polymerization technique [5-6].

This plasma polymerized organic thin films have gained significant interest to the researchers owing to their relative easiness to prepare, their chemical and mechanical stability, their high surface functionalization and their specific optoelectronic properties [7]. The films are typically highly cross-linked, ultra-thin, homogeneous, adherent to the substrate, smooth and pinhole free, inert and insoluble [8-11]. Such unique features render the films appropriate for numerous inflictions including dielectrics for thin film condensers [12-13], protection of semi-conductor devices [14-15], chemically modified electrodes [16-19], scratch resistant coatings for plastic optical components, antireflection coatings [18], protective coatings [12], surface modification for biomedical engineering [20], optical waveguide [21] etc. Hence plasma polymerization should be considered as a method of forming new types of materials rather than a method of preparing conventional polymers. To realize these applications, materials of modified optoelectronic properties such as organic thin films is always being searching by the scientists.

Optical, morphological and electrical properties of plasma polymerized thin films are studied continuously by different researchers still now, because the exact information of the plasma polymerized thin films depended on many parameters such as discharge power, precursor structure, substrate temperature, monomer flow rate, etc. [22], and therefore, those properties can be tuned changing any of the parameters.

The plasma assisted method is the fastest growing area in the field of direct thin film deposition. Day by day there has been growing used of glow discharge plasma to polymerize a variety of organic and organometallic compounds. Therefore, it is of the interest of developing polymer thin films of high quality for a variety of industrial applications. As a consequence, a large number of studies have been performed on the thin polymeric films, yet these materials need further study to find high quality and advanced materials for electrical, electronic, and optical devices in industrial and scientific applications.

In this study 1,2-diaminocyclohexene (DACH) has been chosen as a monomer precursor to deposit plasma polymerized DACH (PPDACH) using both AC (50 Hz) and RF (13.56 MHz) plasma, because, to the best of our knowledge only very few reports on PPDACH thin films are available in the literature. However, so far, no study is found reporting the

optical and electrical properties of the PPDACH thin films and also did not compare the results deposing thin films using both AC and RF plasma. Therefore, PPDACH has been prepared varying different deposition parameters under AC and RF plasma, and surface morphology, structural and optical properties of the thin films are studied with an aim to find their suitable optoelectronic applications, and a comparative study is done on the AC and RF plasma to produce thin films.

1.2 Objectives

From the above discussions, it is expected that the investigation of optical and electrical properties of the plasma polymerized organic thin films of 1,2-diaminocyclohexane (PPDACH) varying the deposition parameters in the AC and RF plasma system will be interesting. The key aim of this research is to prepare smooth, flawless, pinhole-free plasma polymerized 1,2-diaminocyclohexane (PPDACH) thin films to find out different optical parameters and conduction mechanisms in the thin films, and to compare these properties for AC and RF plasma system. The following characterizations have been performed to determine the morphological, structural, thermal, optical and electrical properties of PPDACH thin films of various thicknesses.

(i) Morphological and elemental analysis

Field emission scanning electron microscopy (FESEM), atomic force microscopy (AFM) and energy dispersive X-ray (EDX) analysis have been used to obtain morphological, topographical and compositional information of the PPDACH thin films, respectively.

(ii) Structural analysis

The Fourier transform infrared (FTIR) spectroscopy and X-ray diffraction (XRD) of the samples were recorded to identify different types of bonding vibration and the crystallinity in the films.

(iii) Thermal analysis

Thermal behavior of these samples has been studied by a computer controlled thermogravimetric-differential thermal analyzer (TG/DTA) system.

(iv) Optical properties

To study the different optical properties such as optical band gap, Urbach energy, steepness parameter, absorption co-efficient, extinction co-efficient, refractive index of the deposited PPDACH thin films, UV-visible spectra will be recorded at room temperature using a UV-Visible spectrophotometer.

(v) Electrical properties

The DC electrical measurements will be performed to find out the conduction mechanism in the films.

Finally, the comparison of different properties of the films in the two systems (AC and RF) could give us some new aspects to find their suitable applications in electrical and optoelectronic devices.

1.3 Outline of the Thesis

The thesis paper is divided into five chapters.

Chapter One contains a brief history and potential applications of plasma polymerized thin films. The motivation for the present study is brought out in this chapter.

Chapter Two represents the literature review and theoretical background including the details of plasma, plasma polymerization and its advantages and applications of plasma polymerized thin films, etc. Different experimental techniques used in the various stages of this study such as FESEM, AFM, EDX, FTIR, XRD, UV-Vis spectroscopy, TG/DTA are also briefly discussed in this chapter.

In **Chapter Three**, the experimental details are described. It deals with the preparation of the thin films by AC/RF plasma polymerization, capacitively coupled glow discharge plasma polymerization set up for polymer formation, thin film thickness measurement. The techniques used for characterizing thin films like DTA, TGA, FTIR, FESEM, UV-visible spectroscopy, DC electrical measurements are described in details in this chapter.

Chapter Four represents analyses in details on the morphological, elemental, structural, thermal, optical and current voltage characterization of plasma polymerized thin films. The charge transport mechanisms in plasma polymers are also discussed.

Finally, the findings and further scope of the research are depicted in **Chapter Five**.

CHAPTER 2

LITURATURE REVIEW AND THEORITICAL ASPECTS

2.1 Introduction

The rapid growth of plasma polymerization began in 1960s, particularly in the initial development of the microelectronics industry and the research that led to the hope of using plasma polymer as a dielectric film [23]. Recently, the syntheses of organic thin films have advanced due to their broad applications in mechanics, electronics and optics fields. This chapter represents the literature review and fundamental theories. This chapter also describes various analytical techniques that have been used to characterize the samples at different stages.

2.2 Brief Reviews on Plasma Polymerized Thin Films

Plasma polymerized organic thin films expose fascinating optical and electrical properties suitable for different devices owing to their specific structure, arising from their formation mechanism. Over the years, scientists have been concentrated their research on plasma polymerized organic/organometallic thin films to innovate new materials that have promising properties suitable for the applications of modern science and technologies. A brief review of the researches is given below:

Kamal and Bhuiyan [24] studied the thickness dependent direct current electrical conduction mechanism in plasma polymerized pyrrole (PPPy) monolayer thin films and reported that the current conduction is higher in the films of lower thickness than that of the higher-thickness films at the same voltage and also found space charge limited conduction (SCLC) mechanism (Fig. 2.1 (a)) is dominant in the PPPy thin films thin. This change in the conductivity for different thicknesses suggests a probable change in physical properties during the formation of thin films. In the FRIR spectra (Fig. 2.1 (b)), it is seen that that the spectrum of PPPy is very much different than that of the pyrrole monomer which may be due to the re-organization of monomer during the plasma polymerization.
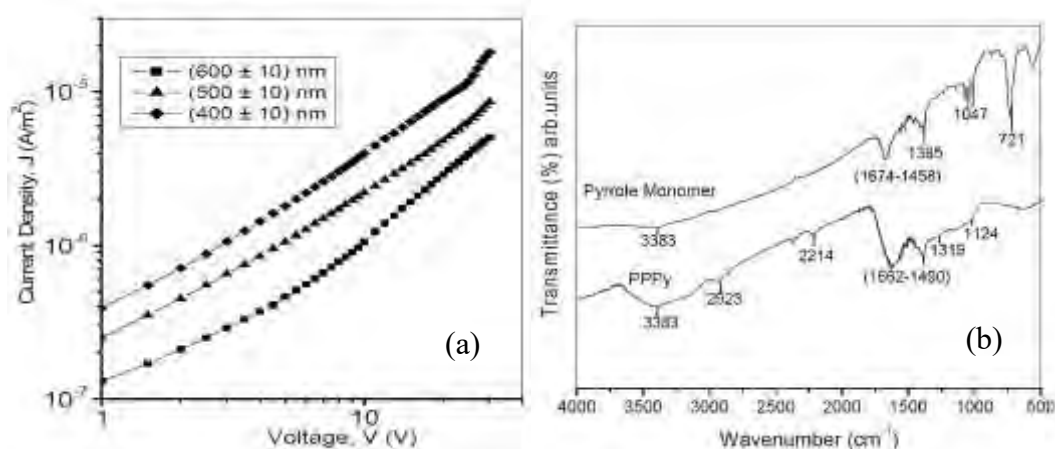
Fig. 2.1: (a) *J-V* characteristics for PPPy thin films of different thicknesses at room temperature, (b) The FTIR spectra of Pyrrole monomer and PPPy [24].

The effect of heat treatment on the optical and structural properties of plasma polymerized 2-(diethylamino) ethyl methacrylate (PPDEAEMA) thin films were investigated by Afroze and Bhuiyan [25]. From SEM analyses (Fig. 2.2), they concluded that the surface of films is smooth, uniform and pinhole free for both the as-deposited and heat treated PPDEAEMA thin films. Both the direct (E_{qd}) and indirect (E_{qi}) band gaps where applicable were decreased with the increase of thickness and are found to be about 3.45–3.25eV and 1.90–1.65eV, respectively because the bulk of the films become more ordered with increasing thickness. It was also observed that the respective E_{qd} and E_{qi} decrease as the temperature increases (Fig. 2.3). The band gap decreases owing to structural rearrangement caused by heat treatment.

Fig. 2.2: The SEM micrographs of as-deposited (a) with magnification 1000×, (b) with magnification 50 000× and (c) heat treated at 573K for 1 h with magnification 50 000×; PPDEAMEA thin films onto glass substrate, at 25 kV [25].
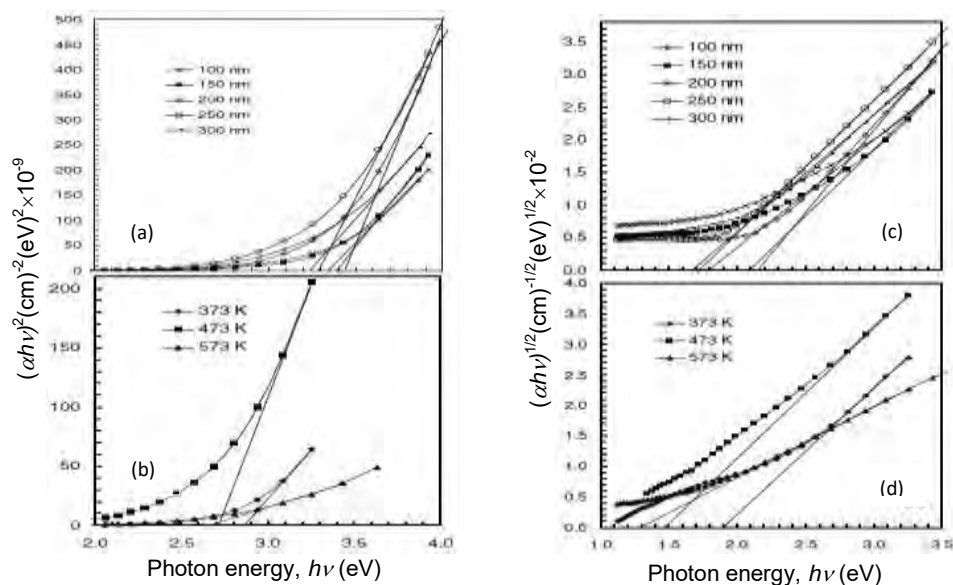
Fig. 2.3: $(\alpha h\nu)^2$ versus $h\nu$ curves for (a) as-deposited, (b) heat treated PPDEAEMA thin films of 150 nm thickness for 1 h and $(\alpha h\nu)^{1/2}$ versus $h\upsilon$ curves for (c) as-deposited and (d) heat treated PPDEAEMA thin films of 150 nm thickness for 1 h [25].

Rahman and Bhuiyan [26] observed structural and optical properties of plasma polymerized *o*-methoxyaniline (OMA) thin films prepared by glow discharge plasma technique. They reported that the surface of the films is uniform, flawless, pinhole free and fracture free as presented in Fig. 2.4 (a-b). FTIR spectroscopy analysis (Fig. 2.4(c)) confirmed that the chemical composition of the PPOMA thin films varies considerably from that of monomer. The absorbance increases with the increase of thickness of the films. The E_{gi} and E_{gd} of PPOMA thin films lie in the range 1.68 to 2.08 eV and 2.90 to 3.08 eV respectively and E_{gd} values of the PPOMA thin films have an increasing trend with the increase of film thickness, whereas E_{gi} values do not depend on the film thickness.

Fig. 2.4: The SEM micrographs: (a) slide view, and (b) cross sectional view of the PPOMA thin films, (c) The FTIR spectra of OMA and PPOMA [26].
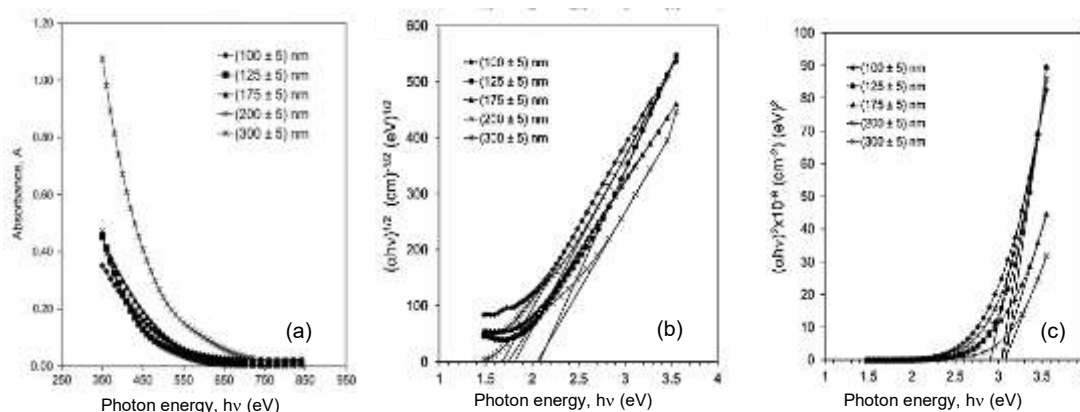
Fig. 2.5: (a) Wavelength versus absorbance plot for different PPOMA thin films, (b) $(\alpha h\nu)^{1/2}$ and (c) $(\alpha h\nu)^2$ as a function of photon energy, hʋ, for PPOMA thin films of different thicknesses [26].

Mechanical and optical properties of fluorine doped silicon oxide (F-SiO$_x$) thin films deposited in a capacitively-coupled radio frequency (RF) (13.56 MHz) PECVD system were studied by Abbasi-Firouzjah and Shokri [27]. They found that the optical and mechanical properties of the deposited films were affected by changing carbon bonds in the films chemical structure due to change of plasma power during polymerization.
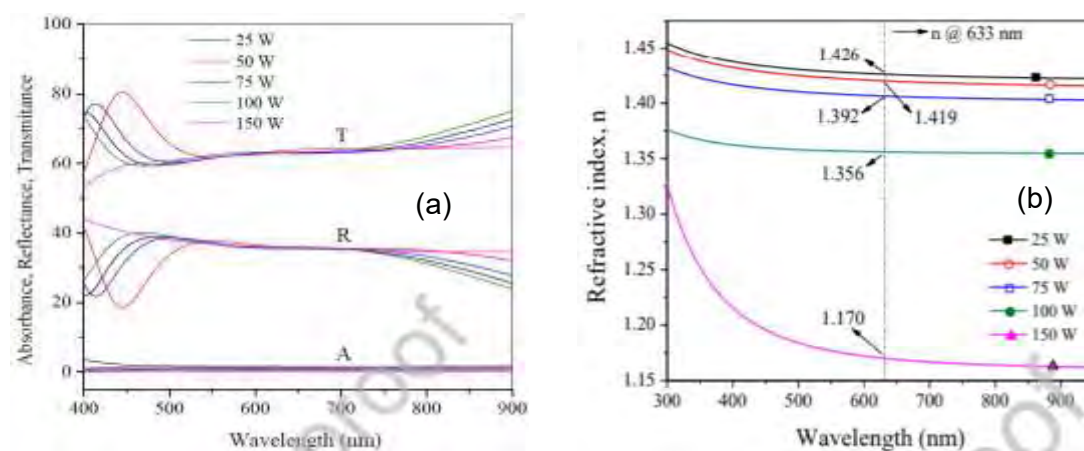
Fig. 2.6: (a) Optical absorbance (A), transmittance (T) and reflectance (R) spectra and (b) Variation of refractive index of F-SiO$_x$ films deposited on silicon substrates as a function of wavelength at different RF powers [27].

It was also shown that decreasing the power applied could result in an increase in the carbon content of the fluorinated silicon oxide film without using additional carbon

precursor. The films are highly transparent and refractive index decreased from 1.426 to 1.170 (at 633 nm) by increasing applied power as shown in Fig. 2.6.

Majumder and Bhuiyan [28] investigated the surface morphology, optical properties and chemical structure of plasma polymerized vinylene carbonate (PPVC) thin films deposited on to glass substrates by low pressure glow discharge plasma at room temperature. SEM micrographs (Fig. 2.7 (a)) of the deposited films show that the surface of the thin films is uniform, flawless, pinhole free and fracture free. The FTIR analyses yields that chemical structure of PPVC thin films slightly different from monomer due to some structural rearrangement during glow discharge (Fig.2.7 (b)). UV-vis spectroscopy shows that the absorbance increases with increasing thickness of the PPVC thin films (Fig. 2.7 (c)). The direct and indirect optical band gaps are found to be in between 3.96 and 4.15 eV for thin film thicknesses between 125 to 200 nm.
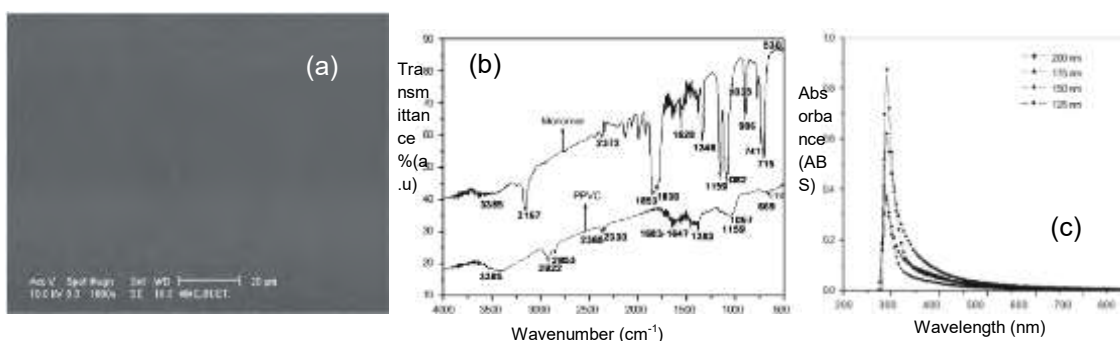
Fig. 2.7: (a) The SEM micrographs of as-deposited PPVC thin films magnification 1000×, (b) The FTIR spectra of monomer VC and PPVC and (c) Variation of absorbance, ABS, with wavelength, λ for PPVC thin films of different [28].

Majumder and Bhuiyan [29] also studied DC conduction mechanism in plasma polymerized vinylene carbonate thin films and concluded that the conduction mechanism is Schottky type.

Sarkar and Bhuiyan [30] investigated DC Electrical conduction mechanism in plasma polymerized 1-Benzyl-2-methylimidazole (PPBMI) thin films fabricated by glow discharge method. They reported that that the chemical structure of PPBMI thin films is changed to some extent from that of the monomer. The analysis of J–V (Fig. 2.8 (a-b)) characteristics

of different thicknesses at various temperatures reveals that space charge limited conduction (SCLC) mechanism is dominant in PPBMI thin films. The activation energy for the conduction mechanism is found to be 0.43 eV. Carrier mobility, free carrier density and trap density are found to be 1.48×10^{-18} to 6.35×10^{-18} m^2 V^{-1} s^{-1}, 1.59×10^{23} to 5.85×10^{23} m^{-3} and 2.50×10^{24} to 5.00×10^{23} m^{-3}, respectively.
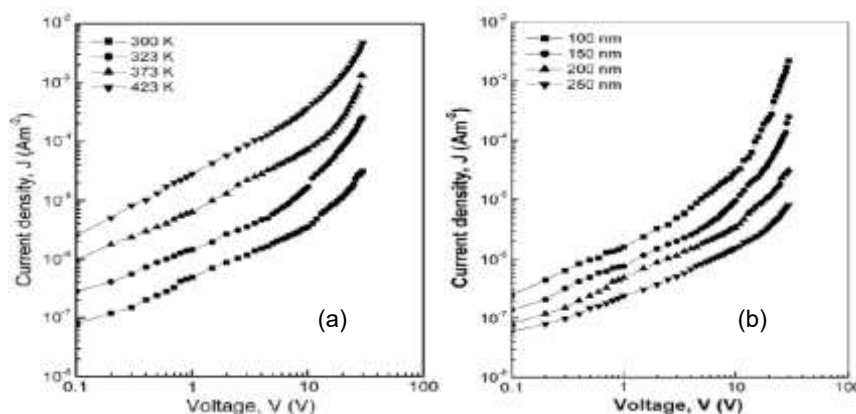
Fig. 2.8: (a) Plots of current density against applied voltage for PPBMI thin films of different thickness at room temperature, (b) Variation of current density with applied voltage at different temperatures for PPBMI thin film (thickness, d =200 nm) [30].

The polymerized cyclohexane thin films were prepared and characterized by Manna et al. [31] using radiofrequency plasma enhanced chemical vapor deposition technique (RF-PECVD) at different radiofrequency powers and a mixture of Argon gas and cyclohexane (C_6H_{12}) vapor was used as the precursor. From AFM topography, the values of surface roughness (R_q) were found equal to 2.67 and 0.35 nm for films deposited at different plasma power. FTIR spectra (Fig. 2.9 (a)) show that increasing the RF power results in a decrease of the intensity of the total band. From the transmittance spectra, they reported that the transmittance is very low in the UV range, is about 40% in the VIS range and it is maximum, of about 80%, in the infrared. The extinction (k) and the absorption coefficients (α) both decrease with the increase of λ but increases with increasing RF power as presented in Fig. 2.9 (b) and (c). Maximum values were found in the UV region and almost vanish in the infrared range which indicates that the films are highly absorbent in the UV range and become transparent in the infrared one. The refractive index increases but the energy band gap is decreasing from 3.76 eV to 2.92 eV with increasing RF power.
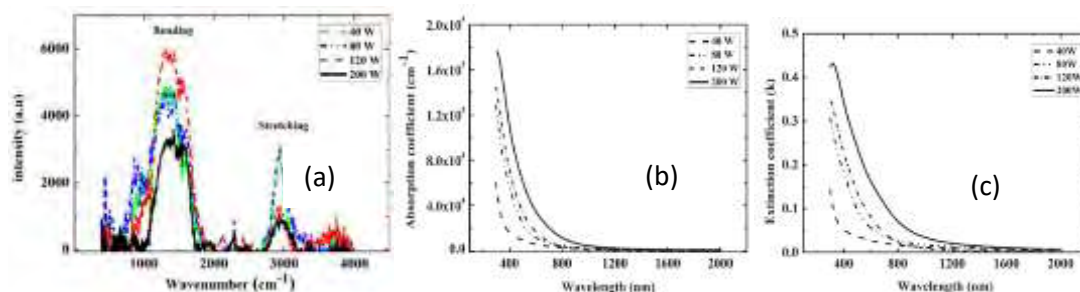
Fig 2.9: (a) Infrared spectra for cyclohexane films deposited at 40, 80, 120, 200W RF power, and variation of the (b) absorption coefficient and (c) extinction coefficient *k* as a function of the wavelength for different RF power [31].

Sanchis et al. [32] observed the effects of low-pressure nitrogen plasma to improve wettability of a polyurethane film surface and studied functionalization /activation phenomena as well as surface roughness changes induced by the plasma-etching mechanism using different techniques.
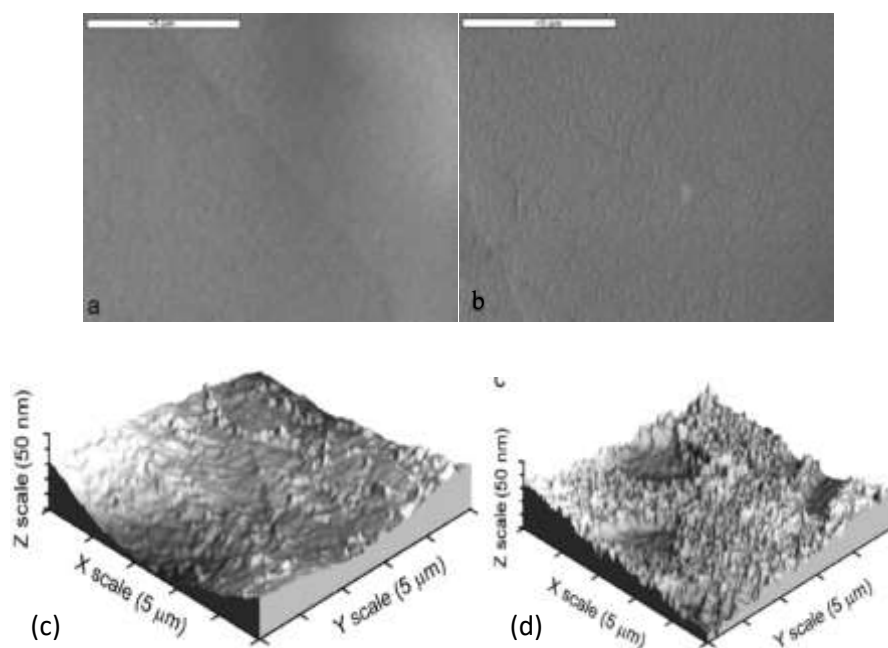
Fig. 2.10: (a) SEM micrographs of polyurethane film with different exposure times to nitrogen plasma (10,000 ×): untreated, (b) 10 min and AFM 3D-topographic images of polyurethane film with different exposure times to nitrogen plasma: (c) untreated, (d) 10 min [32].

The results show a considerable improvement in surface wettability even for short exposure times, as observed by a remarkable decrease in contact angle values. They concluded from SEM and AFM analyses that slight changes occurred in surface topography as shown in Fig. 2.10 (a-d) as a consequence of the plasma-etching mechanism.

Momin et al. [33] studied optical and morphological properties of plasma polymerized cyclohexane (PPCHex) thin films synthesized by using a capacitively coupled parallel plate reactor. They depict that the surface of the PPCHex thin films are smooth, homogenous, uniform and pinhole free which is presented in Fig. 2.11 (a) and (b) and thermogravimetric analyses (Fig. 2.11(c)) reveal that the PPCHx films are thermally stable up to about 510 K. With increasing the thicknesses (d) of the PPCHx thin films from 100 to 550 nm, E_{gd} , E_{gi} and Urbach energy were increased from 2.97 to 3.61 eV, 1.83 to 2.31 eV, and 0.95 to 1.40 eV, respectively.
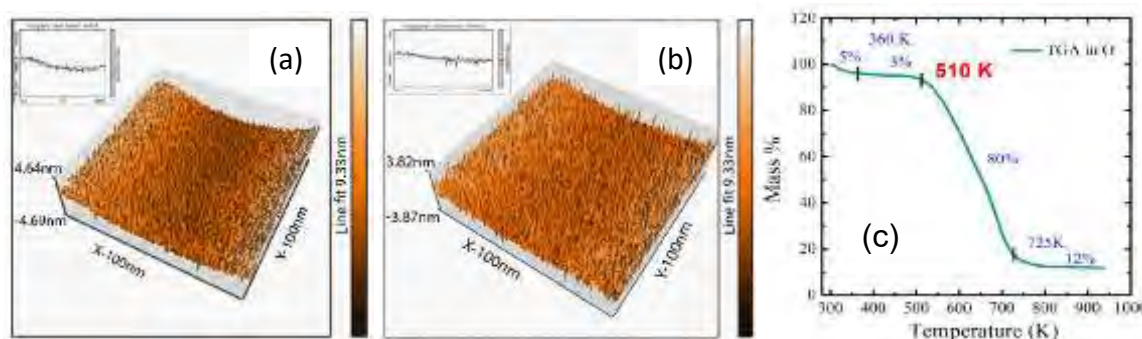
Fig. 2.11: The AFM topography images (3D view) of PPCHex thin films as a function of deposition time, (a) 100 (220 nm) and (b) 110 (350 nm) min (c) TGA thermographs of PPCHex in Oxygen environment (scan rate 10 K/min) [33].

Momin and Bhuiyan [34] also studied DC electrical properties of the PPCHex thin films and reported that the current density increased with increasing temperatures (Fig. 2.12 (a)). Schottky type mechanism was found to be dominant in the conduction mechanism in PPCHex films.
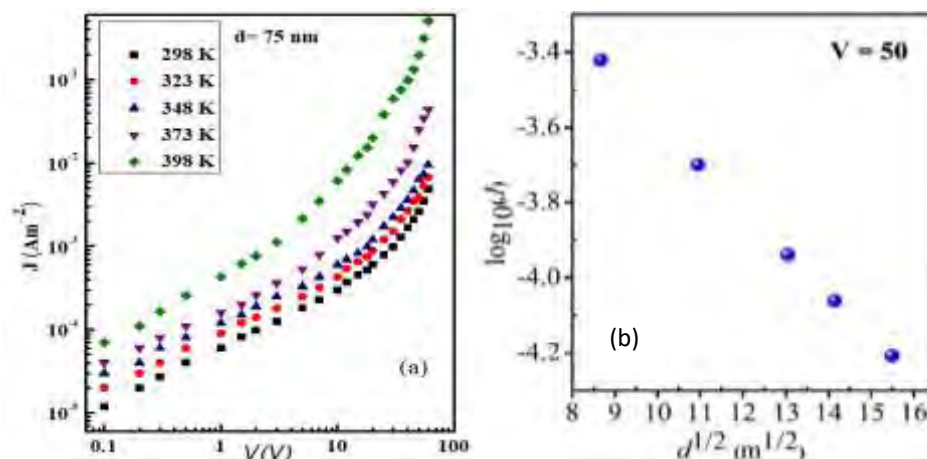
Fig. 2.12: (a) *J-V* plots for PPCHex thin films at different temperature deposited at power 22 W of thickness 75 nm, (b) Plots of $\log_{10} J$ vs $d^{1/2}$ at room temperature for PPCHex thin films deposited at power 22 W in higher voltage region (*J* in Am^{-2}) [34].

Bayram and Simsek [35] were investigated the effect of RF power on the optical, morphological and chemical properties of thin films produced on various substrates using Radio Frequency (RF) plasma polymerization technique from Cinnamaldehyde precursor.
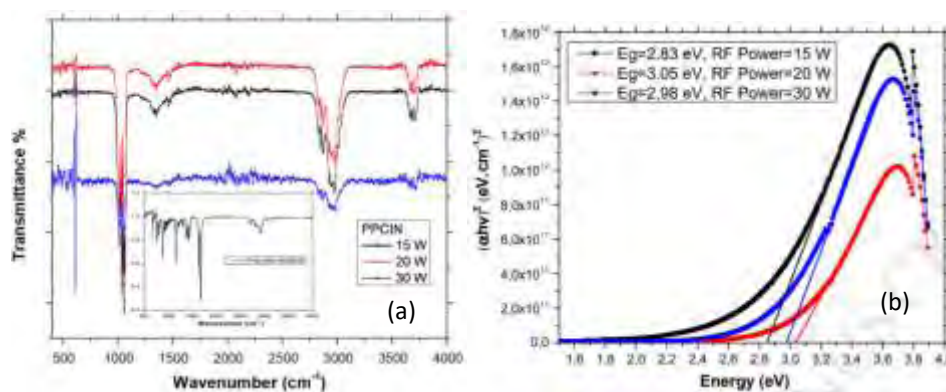
Fig. 2.13: (a) FTIR spectra of monomer material and PPCIN thin films and (b) The plots of $(\alpha h v)^2$ versus energy (*hv*) for PPCIN thin films [35].

The majority of the functional groups belonging to the monomer were mostly preserved in the chemical structure of PPCIN thin films as shown in Fig 2.13. The morphologies of thin films showed a homogeneous and nonporous and radical chain structure. Optical band gap

increased with RF power and the values are lie in between 2.83 – 3.05 eV which indicate that the films have semiconductor properties.

Jatratkar et al. [21] have successfully deposited nanostructured polyaniline (PANI) thin film using glow discharge continuous wave plasma polymerization technique at different RF input power. The input power has a significant effect on the properties of polyaniline thin films. They revealed that the film's refractive index and the surface roughness have been increased whereas the optical band gap and surface energy have been decreased with input power. They confirmed that the surfaces of the films obtained by this method are highly smooth and cross-linked structure as shown in Fig. 2.14 (a-c). The FTIR-ATR (Fig. 2.14 (d)) spectra revealed that all peaks are found at the same position for all input RF powers and the only change is found in their intensity.
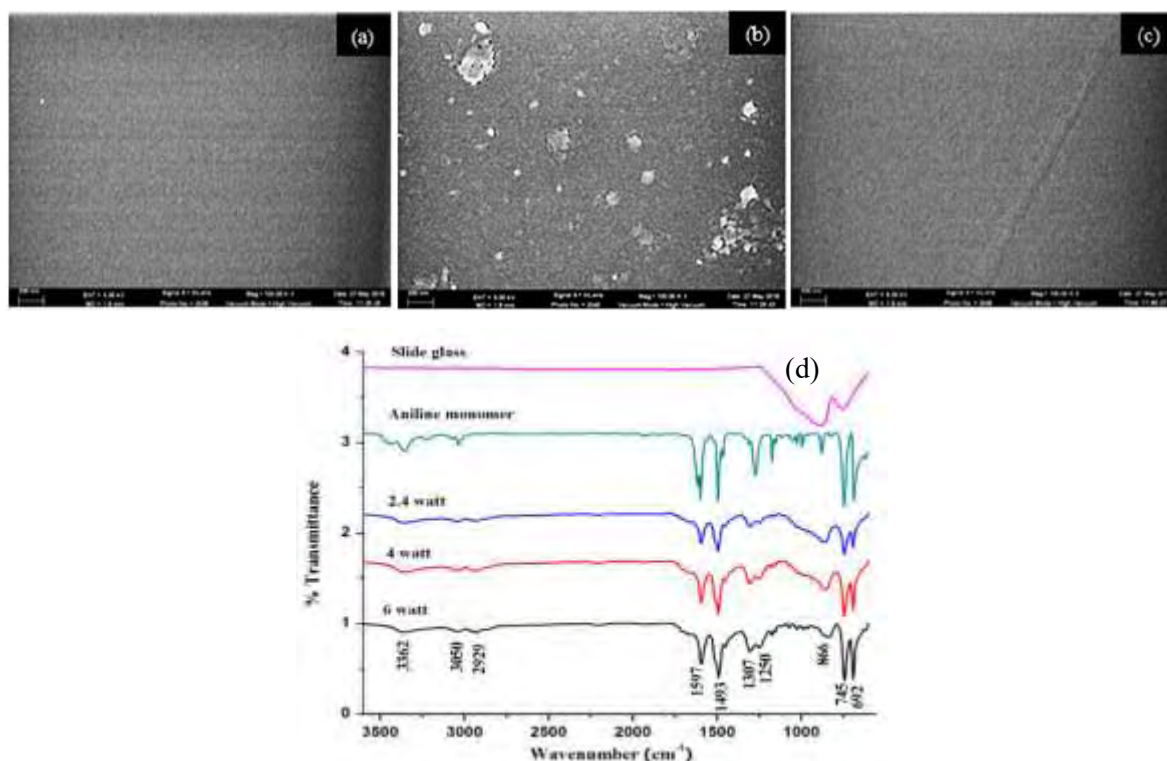
Fig. 2.14: FE-SEM (a, b and c) images of plasma polymerized polyaniline thin film for 6 watt, 4 watt and 2.4 watt input power respectively, (d) FT-IR spectra of plasma polymerized polyaniline thin film for different powers [21].

Golander et al. [36] deposited plasma polymers of three isomers of diaminocyclohexane (DACH) on polyethylene, SiO_2 and investigated the structure and surface properties of DACH plasma polymer thin films. It was observed from FTIR spectra (Fig. 2.15), the NH_2 doublet appearing in liquid 1,2-DACH replaced by a broad peak in DACH plasma polymer film indicating both C-OH and NH functionalities.
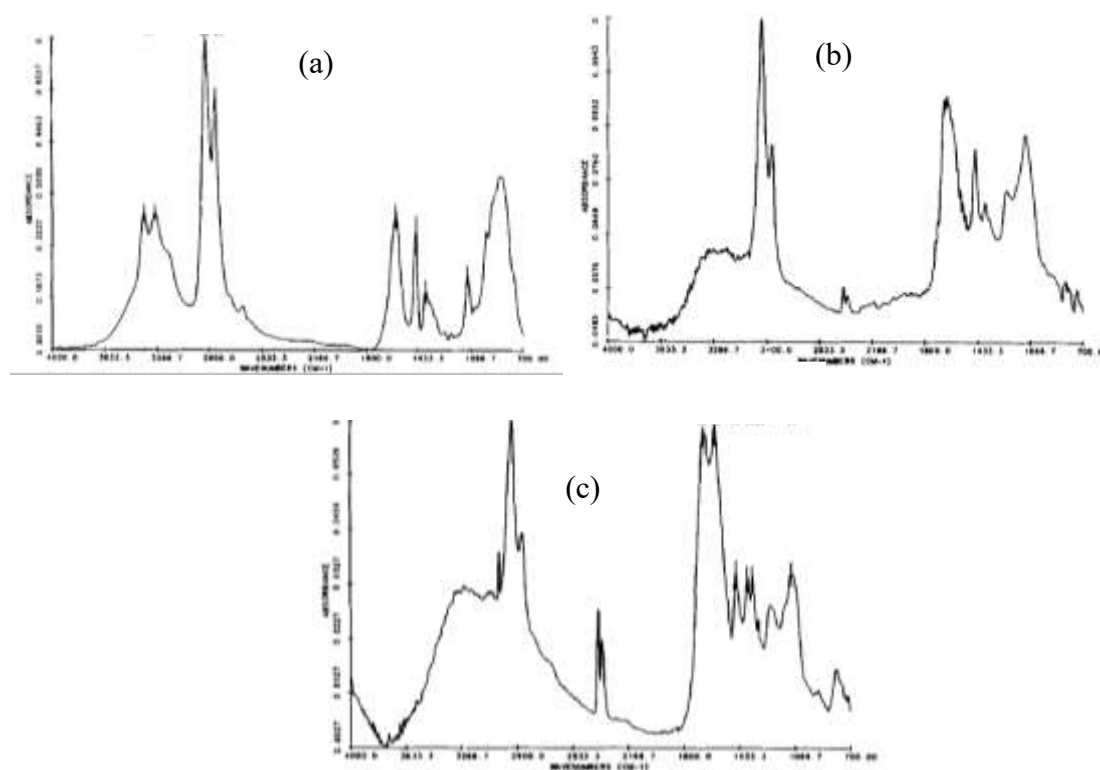
Fig. 2.15: FTIR spectra of 1,2-DACH (a) liquid monomer, (b) 1,2-DACH plasma polymer (PP) film stored for 2 days; (c) 1,2-DACH PP film stored for 18 days [36].

Bae et al. [37] carried out comparative studies on the electrical and optical properties of plasma polymerized organic thin films deposited by PECVD method. From FTIR spectra (Fig. 2.16 (a)) and UV-visible transmittance spectra (Fig. 2.16 (b)), they concluded that as the plasma power was increased, the main IR absorption peak intensity of thin films was increased while the transmittance of the UV–vis spectra was decreased, indicating high cross-linked density. They suggested that their polymer like thin films can be used as insulating materials for microelectronics devices.
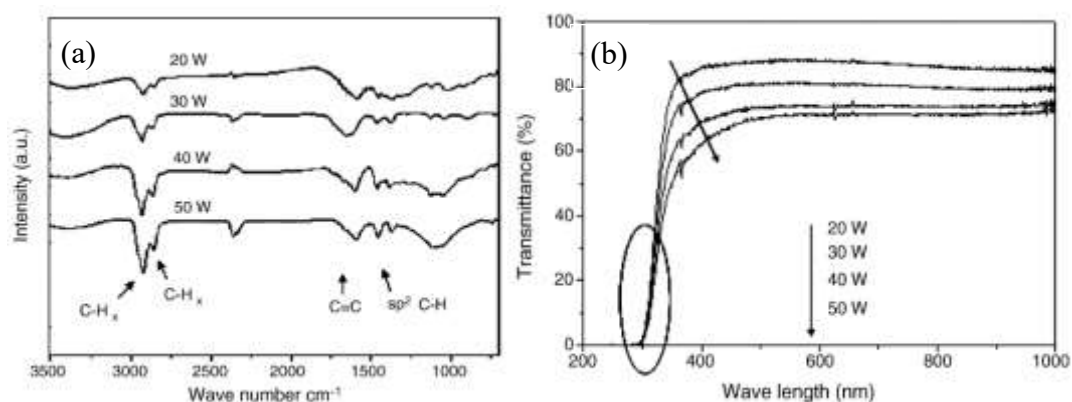
Fig. 2.16: (a) The FT-IR spectra and (b) UV–vis transmittance spectra of methylcyclohexane as-grown thin films at various RF powers. [37].

Shin et al. [38] was successfully immobilized the Bone Morphogenic Protein-2 (BMP-2) on the 1,2-DACH plasma treated Ti surface. The ATR-FTIR results confirmed that BMP-2 could be effectively bounded onto Ti surface via covalent bonding. From AFM images (Fig 2.17 (a-c)), they reported that after DACH plasma treatment, morphological variation was observed very little compared to the untreated Ti surface.
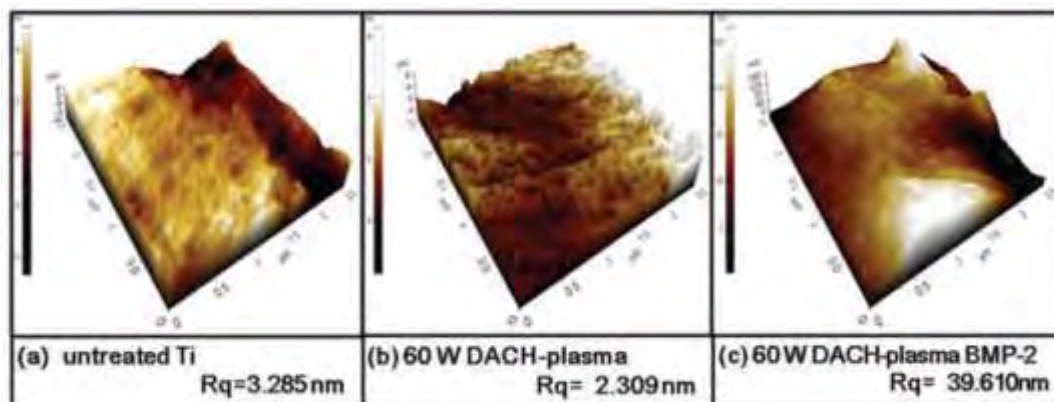
Fig. 2.17: AFM images of Ti and surface modified Ti samples (scale: 2.5 μm×2.5 μm) [38]. The R_q values of untreated Ti and plasma treated Ti samples are found 3.285 and 2.309 nm, respectively, whereas the BMP-2 immobilized Ti surface had a roughness of 39.610 nm. Their research suggests that the DACH plasma polymerized Ti surface has a potential for immobilization of biomolecules in bone tissue engineering.

2.3 Plasma and Plasma Polymerization

2.3.1 Plasma

In 1879, Sir William Crooke first identified "plasma" as a "radiant matter" in a Crooke tube. The American chemist Irving Langmuir first used the term *plasma* (after the Greek word, which means "mouldable substance" or "jelly") to describe an ionized gas in 1920 [39]. More than 99% of matter in the visible universe is thought of plasma. Plasma is considered as fourth state of the matter despite solids, liquids and gases presented in Fig. 2.18. It is a special kind of ionized gas and in general consists of positively charged ions, electrons, and neutrals (atoms, molecules, radicals). Plasma is also defined as the quasi-neutral gas which exhibits a collective behavior [40,41] in the presence of an electromagnetic field.
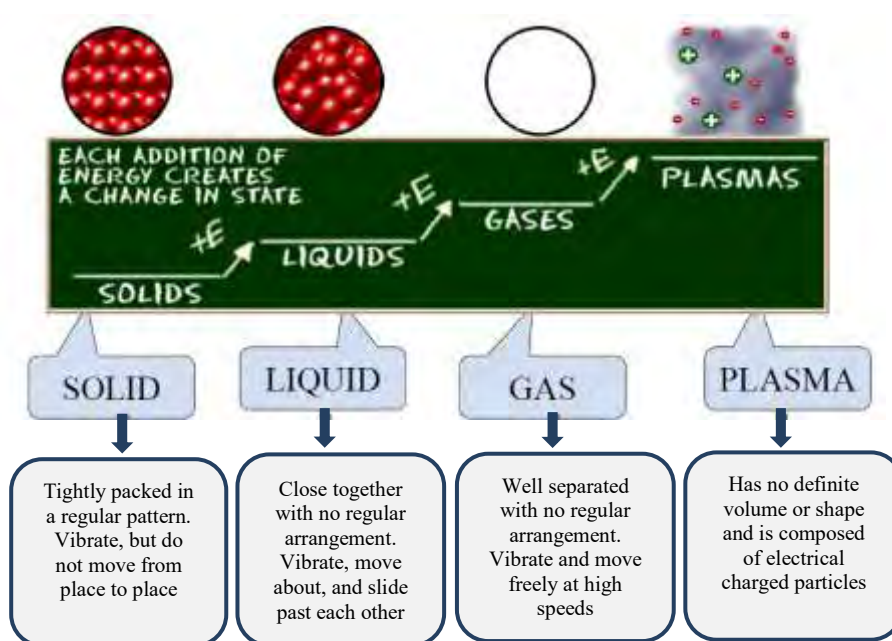
Fig. 2.18: Different states of matter: Solid, liquid, gas and plasma with their physical phenomena [39].

2.3.2 Formation of plasma

Plasma can be created by heating a gas or subjecting it to a strong electromagnetic. Generally, with increasing energy in atoms, the thermal movement of atoms in the solids aggravates and finally overcomes the restrictive interaction between atoms in solid such as ionic bond and forms liquid. If the energy of electron is sufficient to overcome the

electrostatic potential barrier, then the electron is removed to produce a free electron and a positive charged ion. This is known as ionization. Ionization happens many times, creating clouds of free electrons and ions in sufficiently heated gas. This ionized gas mixture consisting of ions, electrons and neutral atoms is called plasma. On average, the plasma is a neutrally ionized gas.

Different techniques like combustion flames, electrical discharges, controlled nuclear reactions, shocks and other means can be used to produce plasma in the laboratory. The technique of most interest is the glow discharge. In glow discharge system, plasmas are produced when energy is transferred by an electric field to free electrons within a low pressure environment. Through inelastic electron collisions with molecules, more electrons, ions, free radicals, and molecules in excited states are generated, and this results in the plasma state. Plasmas produced by this technique are called non-equilibrium or cold plasma. The term non-equilibrium means that electrons and heavy particles are in thermal non-equilibrium [42]. In this case, temperature of the heave particles is much lower than that of the electrons [43]. The heavy particle temperature ranges from 25 °C to 45 °C [44].

2.3.3 Plasma polymerization

Plasma polymerization is a method of formation of polymeric materials under the influence of plasma. Plasma polymerization is the most important technique for fabricating thin polymer films from almost any organic vapor [45,46]. The films obtained by plasma polymerization process are generally chemically inert, insoluble, mechanically tough, thermally stable, and have been used in a wide variety of applications such as selective membranes, protective coatings, electrical, optical, and biomedical films [47-51]. Like conventional polymers, plasma polymers do not consist of chains with a regular repeat unit, but tend to form an irregular three-dimensional cross-linked network. A schematic plasma polymerization configuration is presented in Fig. 2.19 (a). The chemical structure and physical properties may be quite different from the conventional polymer which is derived from the same starting materials. Hence plasma polymerization should be considered as a method of forming new types of materials rather than a method of preparing conventional

polymers. Comparison of the structures of plasma polymers and conventional polymers is shown in the Fig. 2.19 (b).
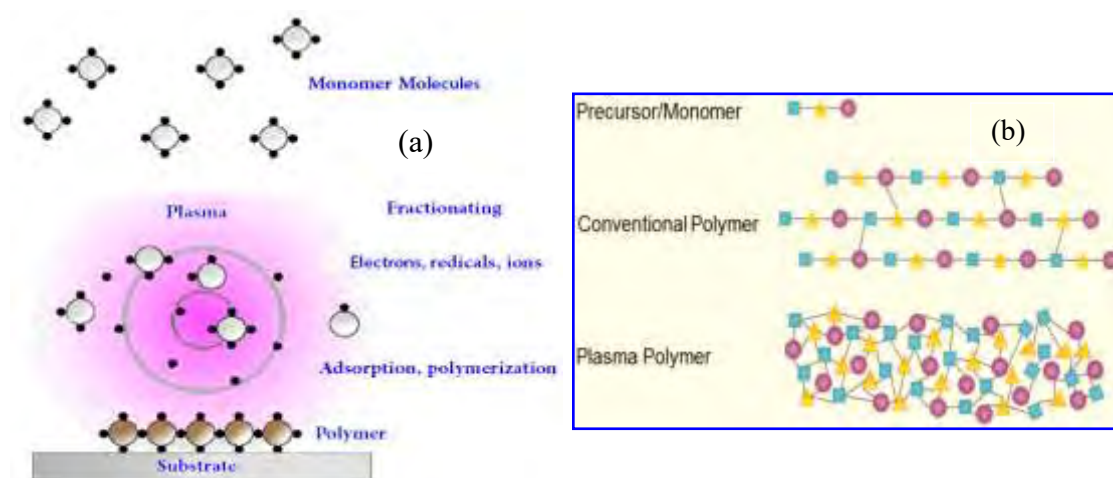
Fig. 2.19: (a) A schematic plasma polymerization configuration and (b) Schematic comparison of the structures of plasma polymers and conventional polymers.

2.3.4 Plasma polymerization process

The mechanism of reaction by which plasma polymerization occurs is quite complex and cannot be specifically described for the general case. Operational parameters such as monomer flow rate, pressure, frequency, and power affect the deposition rate and structure of the plasma film. The electrons or atoms generated by partial ionization of the molecules are the principle sources for transferring energy from the electric field to the gas in all glow discharges [52, 53]. Plasma polymerization process usually takes place in low temperature plasma, which is generated by glow discharges operated in a molecular gas under low pressure. The monomer is converted to a gas in an evaporator and is pumped into a vacuum chamber. Plasma polymerization occurs due to the dissociation of covalent bonds in gas phase molecules, and subsequent reactions between gas phase species and surfaces result in the deposition of polymeric materials. If a strong potential difference between the two electrodes is applied, the gas splits into positive ions and electrons, giving rise to a gas discharge [54, 55].
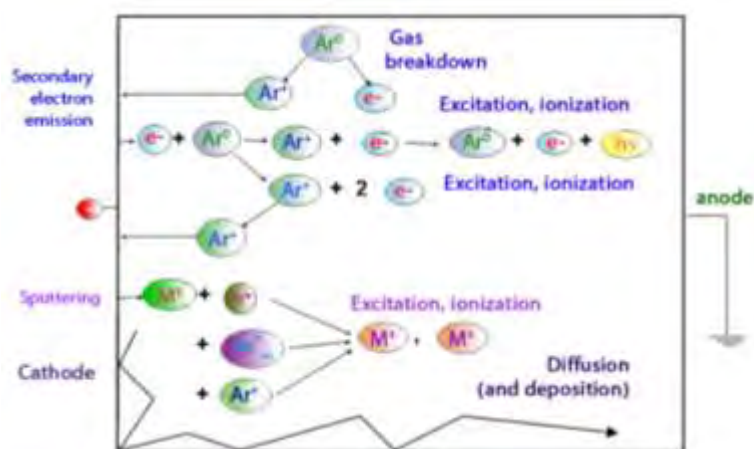
Fig. 2.20: Schematic overview of the basic processes in a glow discharge.

However, when a potential difference is applied the electrons are accelerated by the electric field in front of the cathode and collide with the gas atoms. Inelastic collisions which cause excitation and ionization are the most significant collisions. The ions are accelerated by the electric field toward the cathode, where they release new electrons by ion-induced secondary electron emission. The electrons give rise to new ionization collisions, creating new ions and electrons as shown in Fig. 2.20. These processes of electron emission at the cathode and ionization in the plasma make the glow discharge self-sustaining plasma [44].

2.3.5 Applications of PP thin films

Plasma polymerized thin films have gained considerable significance in many areas of applications such as optics, microelectronics, and biomaterials. Among various uses of PP thin films few potential applications are given below:

❖ In optical systems: Anti-reflection coating, anti-dimming coating, improvement of transparency, optical fiber, optical wave guide, laser and optical window, contact lens, etc.

❖ In electrical devices: Insulator, thin film dielectric and separation membranes for batteries, etc.

❖ In electronic devices: Integrated circuit elements, VLSI resists and in non-crystalline semiconductor and non-crystalline fine ceramic etching, etc.

❖ In chemical processing systems: Protective coating, adhesion improvement abrasion resistant coating, anti-creasing and scratching, etc.

❖ Biomedical applications: Eenzyme immobilization, sustained release of drugs and pesticides, sterilization and pasteurization, artificial kidney, blood vessel, etc.

❖ In textile industries: Anti-flammability, anti-electrostatic treatment, dying affinity, hydrophilic improvement, water repellence, shrink-proofing, etc.

2.4 Synthesis of Thin Films

When a thin layer of solid material is formed on a solid substance and if the layer thickness becomes comparable in magnitude with mean free path of the conduction electrons of solid material this layer is termed as "Thin Film". The limit between "thin" and "thick" films cannot generally be defined, although literature sometimes gives an arbitrary value of 1 μm. Basically, a film can be considered as "thin" when its properties are significantly different from the bulk.

2.4.1 Different techniques of thin film deposition

Thin films can be synthesized by several physical and chemical techniques. The various deposition techniques are shown in Fig. 2.21.
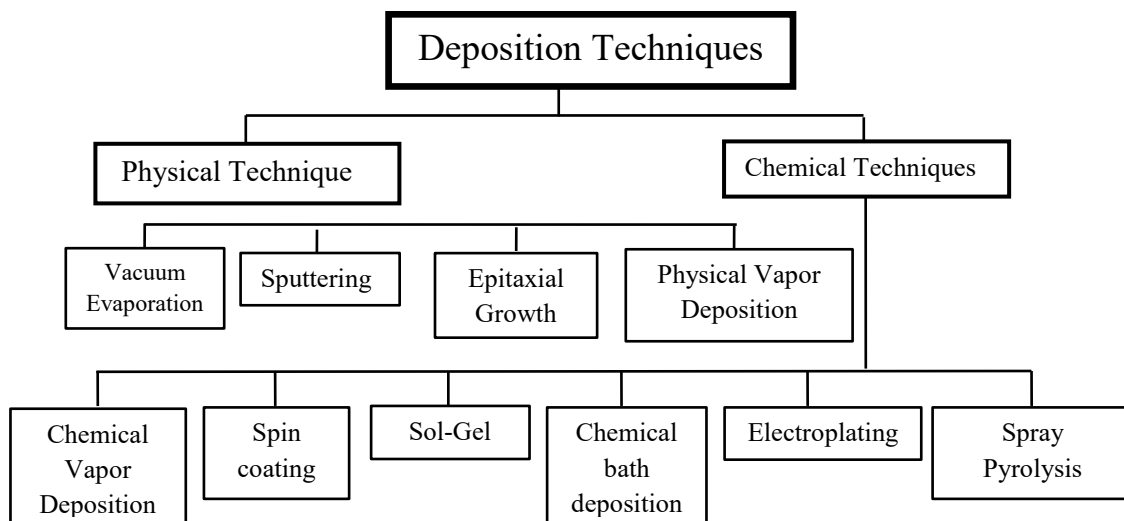
Fig. 2.21: Types of deposition techniques.

2.4.1.1 Chemical vapor deposition (CVD)

Chemical vapor deposition (CVD) is a process used for the synthesis of solid films from a chemically reactive gas mixture. A typical CVD system consists of a gas handling system where precursor is vaporized and injected to reactor vessel where precursors react and an exhaust system where harmful reaction waste products are scrubbed and the harmless gases vented. A schematic diagram of CVD process is shown in Fig. 2.22.
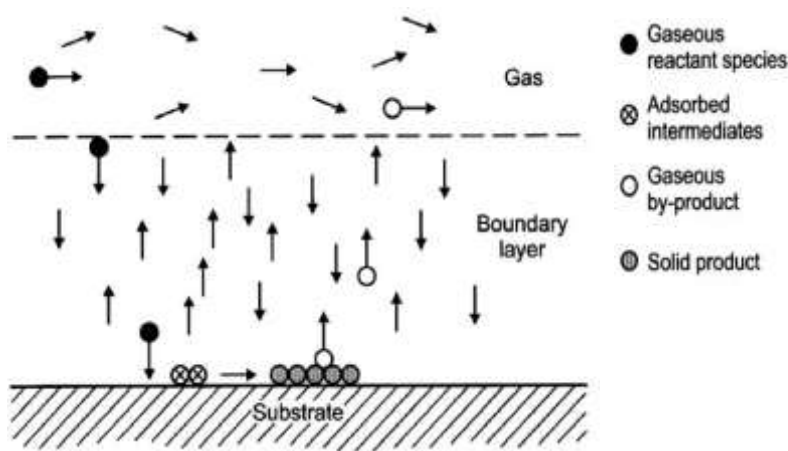
Fig. 2.22: Schematic diagram of a CVD process.

The most important CVD techniques are:

- Metal Organic Chemical Vapor Deposition (MOCVD)
- Plasma Enhanced Chemical Vapor Deposition (PECVD)
- Atmospheric Pressure Chemical Vapor Deposition (APCVD)
- Low Pressure Chemical Vapor Deposition (LPCVD)
- Electron-Cyclotron Resonance CVD (ECRCVD)

In PECVD, deposition rates can be enhanced if the deposition occurs in glow-discharge plasma. Films are deposited from a vapor onto a substrate. Plasma of the reacting gases is created and then several chemical reactions are taking place. In general, the plasma is created by applying discharge power between two electrodes. Fig. 2.23 describes a PECVD process schematically.
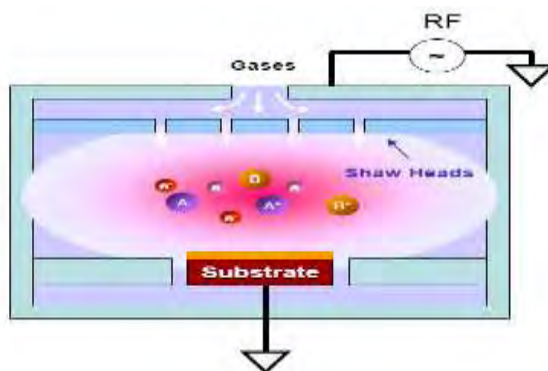
Fig. 2.23: Plasma enhanced chemical vapor deposition process.

2.4.1.2 Physical vapor deposition (PVD)

The Physical vapor deposition (PVD) [56] is a method for depositing thin films on different surfaces by the condensation of a vaporized material. The coating method involves purely physical processes such as high temperature vacuum evaporation rather than involving a chemical reaction at the surface to be coated as in chemical vapor deposition. A typical PVD set up is shown in Fig. 2.24.
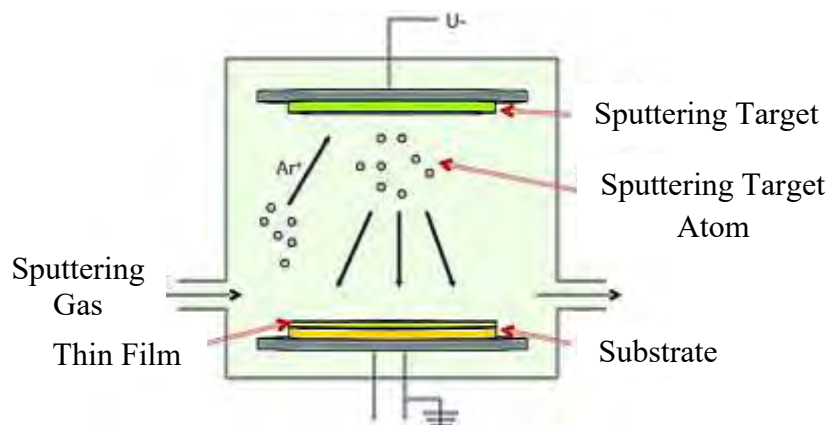
Fig. 2.24: Diagram of physical vapor deposition system [56].

2.5. Theory of Infrared Spectroscopy

Infrared Spectroscopy is an important analytical technique which gives sufficient information about the structure of an organic compound. The absorption of infra-red

radiations can be expressed either in terms of wavelength (λ) or in wave number ($\bar{v}$). Wave-numbers and wavelengths can be inter-converted using the following equation:

$$\bar{v}(cm^{-1}) = \frac{1}{\lambda(\mu m)} \times 10^4 \quad \text{......................} (2.1)$$

It is quite useful to predict the presence of certain functional groups which absorbs at definite frequencies. The absorption of infra-red radiations causes an excitation of molecule from a lower state to the higher vibrational level. All the bonds in a molecule are not capable of absorbing infrared energy but only those bonds which we accompanied by a change in dipole moment will absorb in the infra-red region. It is important to note that since the absorption in infra-red region is quantized, a molecule of the organic compound will show a number of peaks in the infra-red region.

When infrared light is passed through the sample, the vibrational and rotational energies of the molecules are increased. The major types of molecular vibrations are stretching and bending. The various types of vibrations are illustrated in Fig. 2.25 (a) and (b).
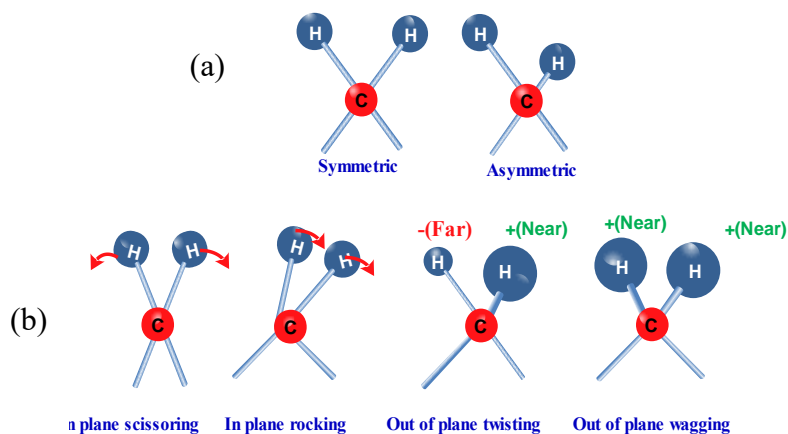
Fig. 2.25: Types of vibrations: (a) Stretching (b) bending.

Stretching: In this type, the movement of the atoms is along the line between them so the interatomic distance is either increasing or decreasing. There are two types of stretching vibrations:

(i)   Symmetric stretching. In this type, the movement of the atoms with respect to a particular atom in a molecule is in the same direction.

(ii)   Asymmetric stretching. In these vibrations, one atom approaches the central atom while the other departs from it.

Bending: In this type of vibrations, the positions of the atoms change with respect to the original bond axis. Bending vibrations are of four types:

(i)   Scissoring. In this type, two-atoms approach each other.

(ii)   Rocking: In this type, the movement of the atoms takes place in the same direction.

(iii)   Wagging: Two atoms move 'up and down' the plane with respect to the central atom.

(iv)   Twisting. In this type, one of the atoms moves up the plane while the other moves down the plane with respect to the central atoms.

2.6 Theory of UV-Visible Spectroscopy

UV-Visible spectroscopy is very useful to measure the number of conjugated double bonds and also aromatic conjugation within the various molecules. Molecules containing π-electrons or non-bonding electrons can absorb the energy in the form of ultraviolet or visible light to excite these electrons to higher anti-bonding molecular orbitals. For visible and ultra-violet spectrum, electronic excitations occur in the range 200-800 nm Due to the quantized energy levels of a molecule, the energy needed for stimulation is a fixed quantity. Therefore, only a particular frequency value of the electromagnetic radiation will be able to cause excitation. When the desired or appropriate frequency radiation is passed, energy will be absorbed and electrons will be impelled to the higher energy states. Therefore, during absorption, light radiation may be either decreased or it can be absorbed completely. As the molecule receives ultraviolet or visible radiation, the electrons are transferred to a higher energy state from the ground state. The important electronic transitions are:

(a) $\sigma \rightarrow \sigma^*$ transitions: This transition occurs in the far UV as it requires a large energy to stimulate an electron from a σ bonding molecular orbitals (MO) to a σ^* anti-bonding MO. This type of transition is possible in saturated hydrocarbons (alkane) where only bonds are formed and no atom has non-bonding electrons. It is a high energy process.

(b) *n→σ** Transitions: Compounds which contain non-bonding electrons (lone pairs) exhibit this type of transition. Organic compounds containing nitrogen, oxygen, sulphur or chlorine have non-bonding electrons. Such transitions require comparatively less energy than that required for σ→σ* transitions.

*(c) π→π** Transitions: this type of transition takes place in unsaturated compounds containing double or triple bonds and also in aromatics. Transition of this type occurs at longer wavelength. For example alkenes, alkynes, carbonyl compounds, cyanides, azo compounds etc. show *π→π** transition. This transition requires still lesser energy as compared to *n→σ** transition and therefore, absorption occurs at longer wavelengths.

*d) n→π** Transitions: This type of transition occurs in compounds containing non-bonding electrons on hetero atom. The electron gets excited to *π** antibonding orbital. This type of transition requires least amount of energy out of all the transitions discussed above and hence occurs at longer wavelengths.
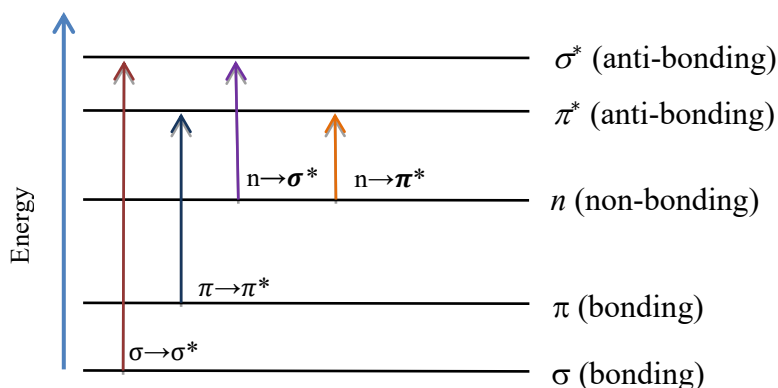
Fig. 2.26: Various transition involved in UV- Vis spectroscopy.

The possible electronic transitions those may be occurred by ultraviolet and visible light absorption are shown in Fig. 2.26. For every possible case, an electron is excited to an empty anti-bonding orbital from a full orbital.

2.7 Theory of DC Electrical Conduction in PP Thin Films

Electrical properties of insulating polymers are there responses when an electric field is applied to them. No known polymer is completely free of conduction processes, however

small the quantity of charge carriers it may possess. Conduction may very often be contributed by impurities that provide a small concentration of charge carriers in the form of electrons or ions. At high fields, the electrodes may inject new carriers (holes and electrons) into polymers. At very high fields, these and other processes will lead to complete breakdown of polymers as insulating materials. The imposition of an electrical field upon a polymer will cause a redistribution of any charges in the polymer, provided they are mobile enough to respond in the time scale in the applied field. A power law can express the variation of current density with voltage in a material generally:

$$J \propto V^n \qquad ………………………..(2.2)$$

Where, n is a power factor. When *n* is unity, the conduction is Ohmic. If the value of *n* is less or more than unity, then the conduction process is other than Ohmic.

Conduction mechanism can be classified into different groups which are shown in the next page.
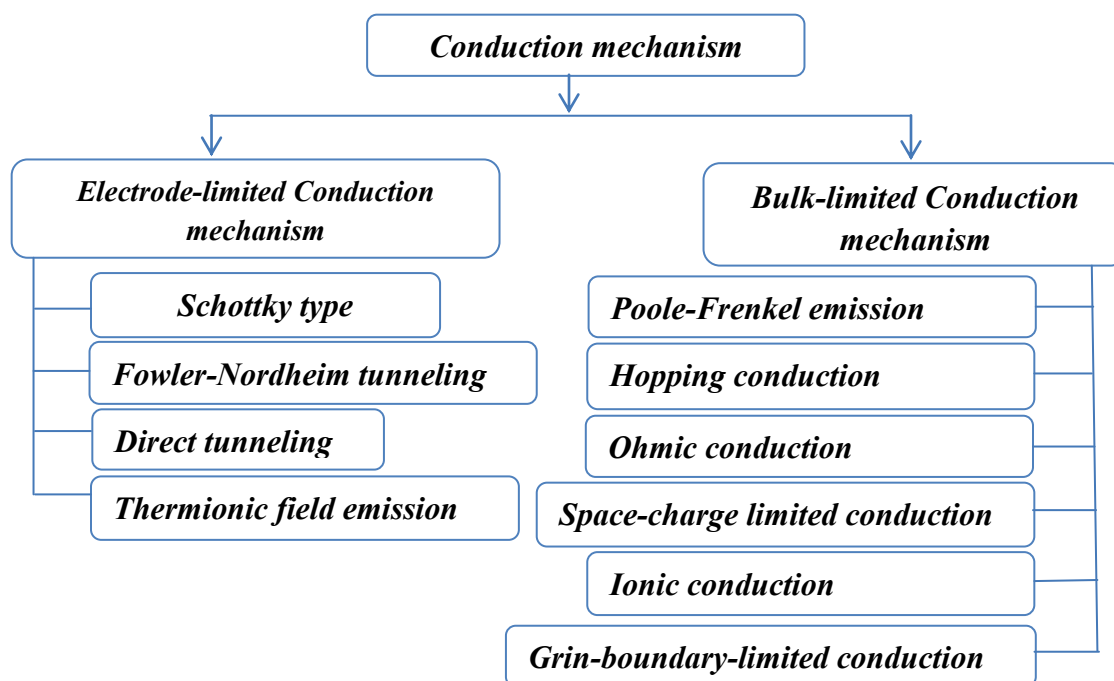
Fig. 2.27: Classification of conduction mechanisms in insulating thin films.

The three most likely mechanisms are thermal or Schottky effect, space-charge-limited conduction (SCLC), and Poole-Frenkel (PF) conduction which are observed in polymer thin films. A brief explanation of these conduction mechanisms is stated below:

(i) Schottky or thermionic emission

Schottky emission is a conduction mechanism that if the electrons obtain enough energy provided by thermal activation, the electrons in the metal will overcome the energy barrier at the metal dielectric interface to go to the dielectric. The energy barrier height at the metal dielectric interface may be lowered by the image force. Fig. 2.28 shows the energy band diagram of Schottky emission in MIM structure. The barrier-lowering effect due to the image force is called Richardson-Schottky (RS) or Schottky effect [57]. The potential energy, φ_{im} of the electron due to the image force is

$$\varphi_{im} = \frac{e^2}{16\pi\varepsilon_0\varepsilon'x} \quad \ldots\ldots\ldots\ldots \text{(2.3)}$$

$$x_m = \left(\frac{e}{16\pi\varepsilon'\varepsilon_0 F}\right)^{1/2} \quad \ldots\ldots\text{(2.4)}$$

where x_m is the distance of electron from the electrode surface, ε' is the high frequency dielectric constant of the material. The change in the barrier height due to the interaction with the image force is given by

$$\Delta\phi_s = \left[\frac{e^3}{4\pi\varepsilon'\varepsilon_0}\right]^{1/2} F^{1/2} = \beta_s F^{1/2} \ldots\ldots\ldots\ldots\ldots\text{(2.5)}$$

where, $\beta_s = \left(\frac{e^3}{4\pi\varepsilon'\varepsilon_0}\right)^{1/2}$ is known as Schottky coefficient.

Current density J can be expressed as,

$$J = AT^2 \exp\left(\frac{\beta_s F^{1/2} - \varphi_0}{K_B T}\right) \ldots\ldots\ldots\ldots\ldots\text{(2.6)}$$

where, φ_0 is the neutral barrier height .

In Schottky mechanism the current density J has an exponential dependence of the square root of the applied field.
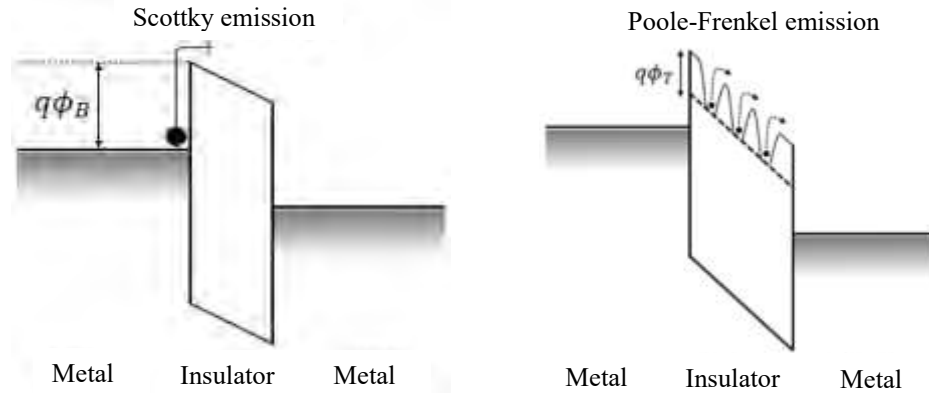
Fig. 2.28: Schematic energy band diagram of (a) Schottky and (b) Poole-Frenkel emission in MIM structure [57].

(ii) Poole-Frenkel emission

When an electric field is applied to a sample, the potential barrier height caused by Coulombic forces of an atom will be reduced. This phenomenon is known as the Poole-Frenkel (PF) effect [57]. The reduction in potential energy may increase the probability of an electron being thermally excited out of the trap into the conduction band of the dielectric. The PF lowering of a Coulombic barrier $\Delta\phi_{PF}$ in a uniform electric field is twice that due to the Schottky effect at a neutral barrier, because the potential energy of an electron in a Coulombic field $-\dfrac{e^2}{4\pi\varepsilon_0\varepsilon x}$ is four times that due to image force effects in Schottky mechanism; i.e.,

$$\Delta\phi_{PF} = 2\Delta\phi_s = 2\left(\frac{e^3}{4\pi\varepsilon'\varepsilon_0}\right)^{1/2} F^{1/2} \equiv \beta_{PF}F^{1/2} \quad \ldots\ldots\ldots\ldots\ldots\ldots(2.7)$$

where, β_{PF} is PF coefficient.

From this we can conclude that, $\beta_{PF} = 2\left(\dfrac{e^3}{4\pi\varepsilon'\varepsilon_0}\right)^{1/2} = 2\beta_s$

i.e., $2\beta_S = \beta_{PF}$ …………………………..(2.8)

In the bulk limited PF mechanism, the thermal emission of trapped carriers from the bulk material gives rise to conductivity

$$J = \sigma_0 F \exp\left(\frac{\beta_{PF}F^{1/2} - \phi_c}{kT}\right) \quad ………………(2.9)$$

where, ϕ_c is the ionization potential of the PF centers.

Consequently, a general expression of the form

$$J = J_0 \exp\left(\frac{\beta F^{1/2} - \phi}{kT}\right) \quad ………………..(2.10)$$

holds equally well for both Schottky and PF mechanisms. Where, J_0 is the current density at a biased voltage. The plot of log J vs. $V^{1/2}$ will give is a straight line and generally referred to as a Schottky plot.

By taking natural logarithms of Eq. 2.10 we can write,

$$\beta_{exp} = SkTd^{1/2} \quad …..............................(2.11),$$

where, β_{exp} denotes the value of β obtained experimentally and $S\left(=\frac{\Delta \ln J}{\Delta V^{1/2}}\right)$ is the slope of ln J vs $V^{1/2}$ graph. Comparison of the theoretical and experimental values of the β coefficient distinguishes between Schottky and Poole-Frenkel mechanism.

(iii) Space-charge-limited conduction (SCLC)

When an Ohmic contact is made to the insulator, the space charge injected into the conduction band of the insulator is capable of carrying current and when the transport is slower than generation, it constitutes the rate-determining step, and the conduction is described by the theory of SCLC [58]. At higher voltages the *J-V* characteristic can be described by the Mott-Gurney relation.

$$J = \frac{9\mu\varepsilon'\varepsilon_0 V^2}{8d^3} \quad \ldots\ldots\ldots\ldots \ (2.12)$$

where, μ is the mobility of charge carriers, ε is dielectric constant, ε_0 is the permittivity of free space, V is the applied voltage and d is the thickness. From the slope of the log J-log V plot, we can observe that J depends quadratically on V. Furthermore, differentiation between the types of the electronic conduction can be done by investigating the dependence of J on film thickness, d ($J \propto d^{-l}$) for the samples of different thickness at a constant voltage, where l is the parameter dependent on the trap distribution within the material. A slope $l < 3$ is indicative of PF or RS conduction, while $l \geq 3$ indicates the possibility of SCLC.

CHAPTER 3

MATERIALS AND METHOD

3.1. Introduction

This chapter deals with plasma polymerization process and provides information about monomer, substrate and capacitively coupled glow discharge plasma polymerization set up for polymer formation. The techniques used for characterizing thin films like DTA, TGA, FTIR, FESEM, UV-visible spectroscopy, DC electrical measurements are described in details.

3.2 Monomer

The monomer 1,2-diaminocyclohexane (DACH), mixture of cis and trans used as precursor in this research. The chemical structure of the monomer precursor, DACH ($C_6H_{14}N_2$) purchased from Sigma-Aldrich. Germany is shown in Fig. 3.1. The physical and chemical properties of 1,2-diaminocyclohexane are described in Table 3.1
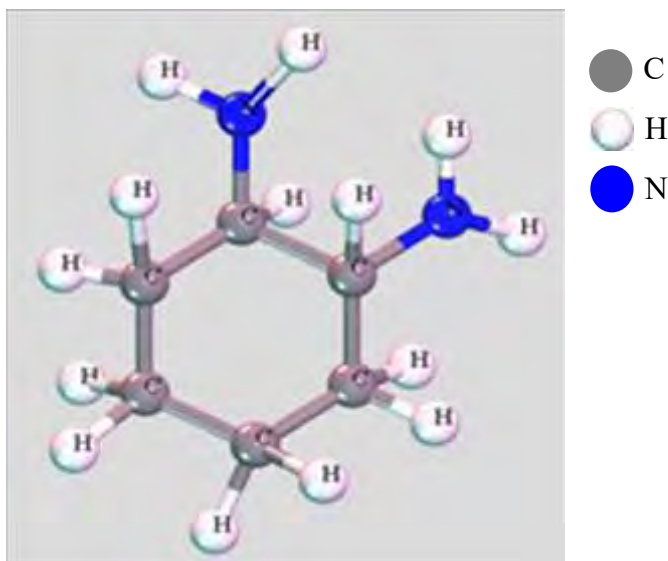
Fig. 3.1: Chemical structure of 1,2-diaminocyclohexane.

Table 3.1: General properties of 1,2-diaminocyclohexane.

IUPAC name	1,2-diaminocyclohexane
Molecular formula	$C_6H_{14}N_2$
Physical state	Liquid
Color	Yellowish liquid
Toxicity	Non-toxic
Molecular weight	114.192 g/mol
Boiling point	183 °C at 76 mm Hg
Density	0.931 g/mL at 25 °C
Vapor pressure	0.4 mm Hg (20 °C)
Refractive index	1.49

3.3 Substrate and Its Cleaning

Glass slides (dimension: 25.4 mm × 76.2 mm × 1.2 mm) of Sail brand, China, purchased from local market. It is essential to make the surface of substrate as clean as possible using acetone and distilled water in an ultrasonic bath to obtain a homogeneous, smooth and flawless thin polymer film, which is a common property of plasma polymers. The clean glass slides were subsequently rinsed with de-ionized water and then dried by a drier.

3.4 Plasma Polymerization Set-up and Deposition Process

The PPDACH thin films were deposited using a homemade and capacitively coupled parallel plate (CCP) reactor (18 cmϕ × 15 cm). Figure 3.2 represents the schematic diagram of the plasma polymerization set up. The reactor consists of parallelly placed two circular plates of diameter and thickness 0.1 m and 0.001 m, respectively, separated by a distance of 0.04 m, along with other important components as illustrated in the figure. The pre-cleaned substrates were kept on the lower electrode. A rotary pump was used to pump down the reactor chamber up to 0.1 Torr very slowly. Glow discharge plasma was generated powering the two parallel plates using AC (50 Hz) and RF (13.56

MHz). When the desired plasma glow in the reactor is shown the monomer vapor produced through heating the liquid DACH using hair drier is injected into the plasma reactor to obtain the PPDACH thin films. The monomer flow rate (20 cm³/min) was adjusted by a fine injection valve in such a way that working pressure during deposition remains stable at about 0.3 Torr.

1. High voltage power supply
2. High tension leads
3. Monomer injection valve
4. Flow meter
5. Monomer container
6. Pyrex glass dome
7. Electrodes
8. Electrodes stands
9. Gasket
10. Lower flange
11. Bottom flange
12. Brass tube
13. Valve
14. Pirani gauge
15. Filter
16. Rotary pump
17. Switch
18. Variac
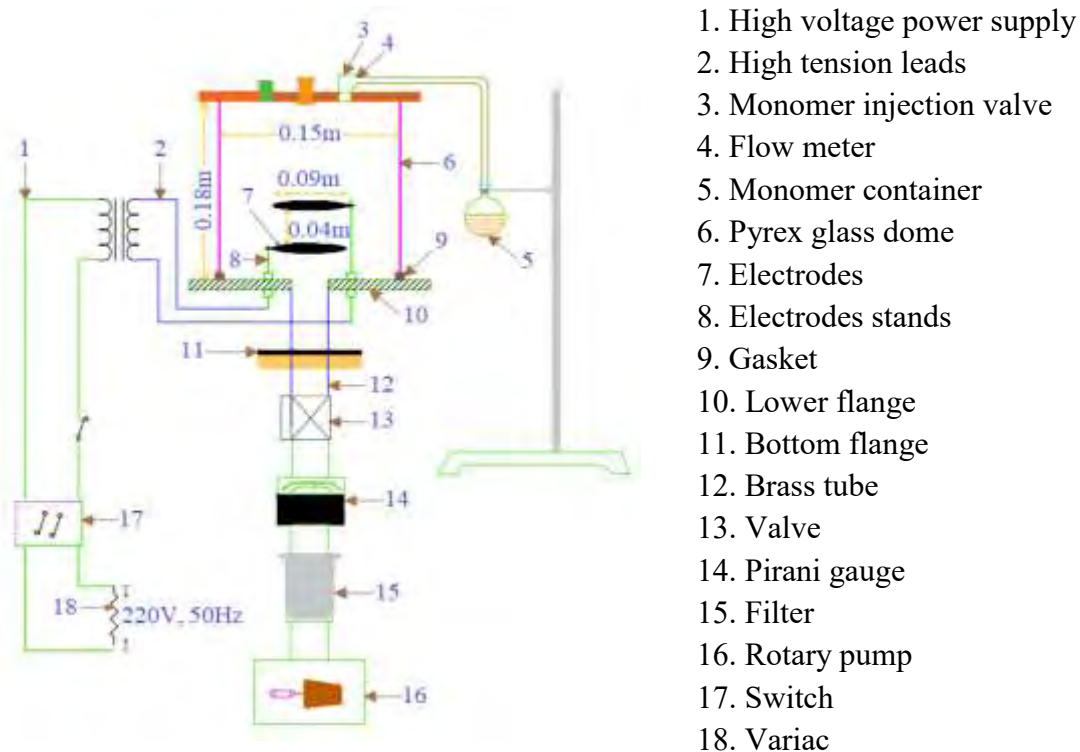
Fig. 3.2: Schematic diagram of glow discharge plasma polymerization set-up.
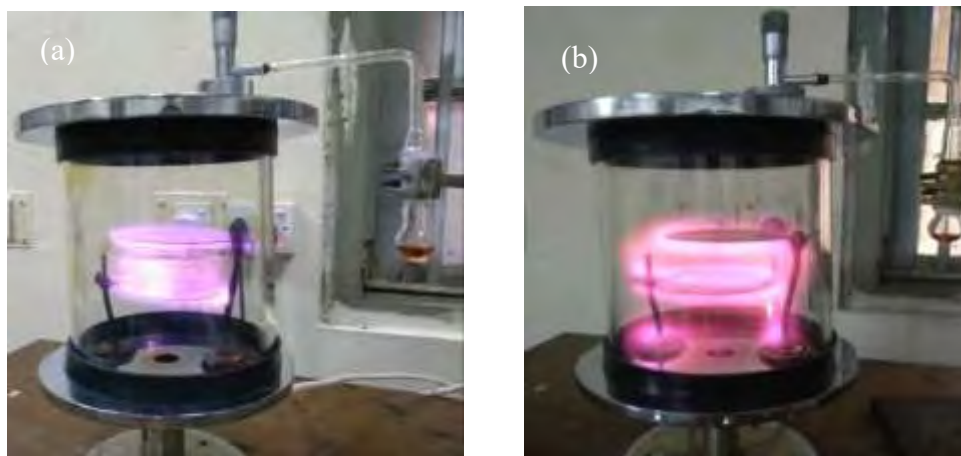
Fig. 3.3 Glow discharge plasma during deposition (a) AC plasma and (b) RF plasma.

Incorporation of monomer vapor in the chamber changed the usual color of plasma into a light violet and light pinkish color for AC and RF power source as shown in Fig. 3.3 (a) and (b), respectively. The deposition time was varied from 30-150 minutes in order to obtain PPDACH thin films of varying thicknesses at a constant AC and RF discharge power of 40 W and 90 W, respectively.

In the present study, optimization conditions for thin film formation are as follows:

Table 3.2: Optimized conditions for thin film deposition.

Experimental condition	Name/Values	
	AC plasma	RF plasma
Electrode distance	4 cm	4 cm
Position of the substrate	Lower electrode	Lower electrode
Deposition power	40 W	90 W
Pressure before deposition	0.1 Torr	0.1 Torr
Pressure during deposition	0.3 Torr	0.3 Torr
Deposition time	30-150 min	30-60 min
Frequency	50 Hz	13.56 MHz

3.5 Thickness Measurement

Thickness of a thin film, which is coated on a substrate, is very important because the film's properties are largely dependent on its thickness In this work, the thickness of the deposited films were measured with the help of a multiple beam interferometric technique according to Tolanskey [59]. This method is the most widely used and in many respects also the most accurate and satisfactory one [59]. The principle of FI is based on separated amplitude interference [60, 61]. Form the principle of Fizeau fringe, the thickness of the film "d" can be determined by the relation

$$d = \frac{\lambda}{2} \frac{b}{a} \quad \text{……………………….. (3.6),}$$

where, λ is the wavelength and $\dfrac{b}{a}$ is the fractional discontinuity identified in the Fig. 3.4. In general, the sodium light is used, for which $\lambda = 589.3$ nm.

A schematic diagram of the multiple-beam interferometer along with a typical pattern of Fizeau fringes from a film step and Fizeau fringe pattern observed during thickness measurement are shown in Fig. 3.4.
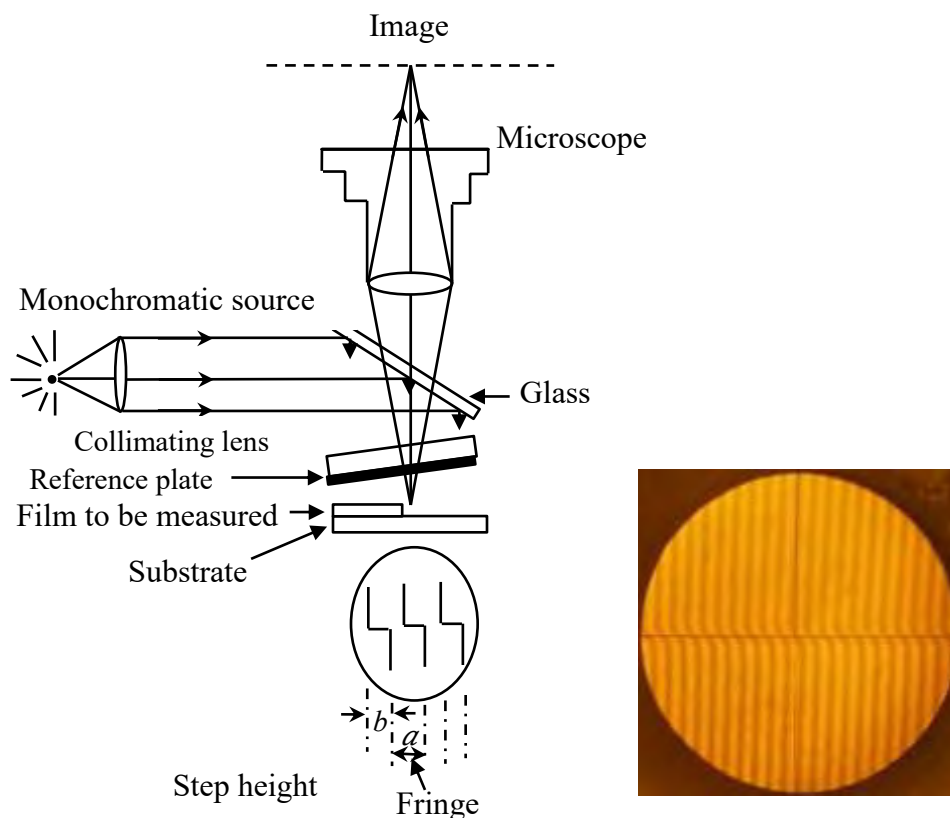
Fig. 3.4: Diagram of Fizeau interferometer used for the measurement of thin film thickness (Inset: Fizeau fringe pattern of the PPDACH thin films).

3.6 Electroding Process

Aluminium (Al) (purity of 4N British chemical standard) was used for electrode deposition. It has been documented that Al has strong adhesion with glass slides [62]. Al film has the benefit of easily self-healing burn out of flaws in sandwich structure [76]. Electrodes have been deposited using a Hind High Vacuum coating unit (Model - 12A4D, India). The system was evacuated by an oil diffusion pump backed by an oil

rotary pump to a pressure less than 10^{-5} Pa. The glass substrates with mask were supported by a metal rod 0.1 m above the tungsten filament and Al was kept on the tungsten filament. The filament was heated by low-tension power supply which can produce 100 A current at a potential drop of 10 V.

Left .... **Right** (a)

Lower electrode .... Lower electrode

Left .... **Right** (b)

Lower electrode ..... Lower electrode and sample .... Sample

Right (c)

Left

Lower electrode .... Sample in between lower and upper electrode .... Upper electrode .... Sample
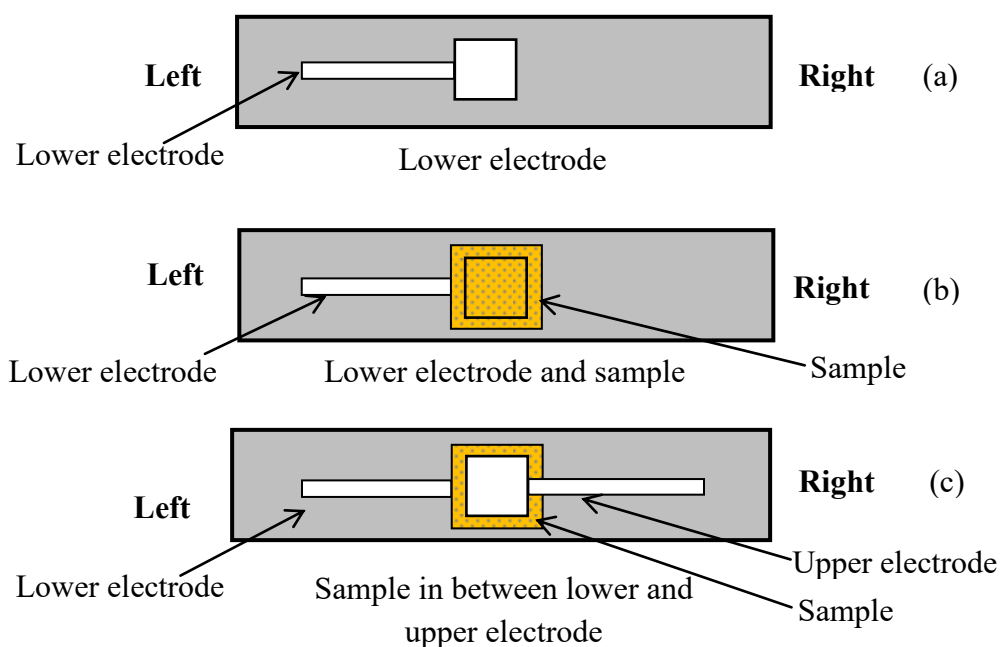
Fig 3.5: Electrode assembly: (a) Lower electrode, (b) lower electrode and the sample, (c) sample in between the lower and upper electrode

The water continuously flowed in order to cool the diffusion unit. After evacuating about 10^{-5} Pa, the Al was heated until it was melted by low-tension power supply. The Al was evaporated, thus lower electrode onto the glass slide was deposited. Al coated glass substrates were taken out from the vacuum coating unit and were placed on the middle of the lower electrode of the plasma deposition chamber for 1,2-diaminocyclohexane thin film deposition under optimum condition. The top Al electrode was also prepared on the PPDACH film as described in Fig. 3.5.

3.7 Characterization Techniques

In this work, the plasma polymerized thin films have been characterized by different experimental techniques. The techniques are given below:

3.7.1 FESEM and AFM

A FESEM (Model JEOL JSM 7600F, USA) was used to observe the surface morphology of the prepared thin films. In order to prevent the charging effect during FESEM, the PPDACH thin films were covered with a thin layer of gold by the assistance of a gold sputtering coater. The compositional elements of the films have also been confirmed by EDX analyses attached to the FESEM. Surface homogeneity of the films also has been observed by a Nanosurf AG, C3000 Flex AFM (Switzerland), where the microscope was performed in a non-contact tapping mode.

3.7.2 Fourier transforms infrared spectroscopy

To elucidate chemical structure of the DACH and PPDACH, FTIR spectra of the liquid monomer and the polymer thin films in the powder form (which is collected from the substrate by scrapping method) have been taken in the wavenumber range of 400 – 4000 cm^{-1} using a double beam spectrometer (FMR- 400 Spectrophotometer, Shimadzu, Japan).

3.7.3 X-ray diffraction

The crystallinity of the films was investigated from XRD pattern of the films taken by an X-ray diffractometer (BRUKER, D8 ADVANCE) using CuK$_\alpha$ ($\lambda = 1.5406$ Å) radiation.

3.7.4 UV-Vis spectroscopy

The optical absorbance measurement of the PPDACH thin films deposited onto glass substrates was recorded by a double beam UV-Vis spectrophotometer (Shimadzu UV-1601, Japan) in the wavelength range of 300 – 800 nm and that was used to obtain the

optical bandgap energy and other various important optical parameters such as absorption coefficient, extinction coefficient, Urbach energy, steepness parameter, refractive index, etc. During the measurement, a similar blank glass slide was used as a reference.

3.7.5 Differential thermal and thermogravimetric analysis

In order to investigate the thermal stability of the PPDACH thin films, thermogravimetric analysis (TGA) was carried out by a computer-controlled TG/DTA 6300 systems linked to a EXSTAR 6000 station. The TGA/DTA model uses a horizontal system balance mechanism. The heating rate was 20 K/min in nitrogen. Alumina was used as the reference medium throughout the tracing process.

3.7.6 DC electrical measurement

For DC electrical measurements, sandwiched type Al/PPDACH/Al samples were formed by using a metal coating unit (Edward 306, England, UK) at a pressure of about 1.33×10^{-3} Pa with an effective Al electrode area of 10^{-4} m^2. The current across the thin films was measured by a high impedance electrometer (Model: 614, Keithley Instruments Inc., USA) and DC voltage was supplied a stabilizer DC power supply (Model: 6545A, Agilent, Japan). The DC measurements were performed at different constant temperatures (298, 323, 348, 373 and 398 K). The temperature of the samples was recorded by a Chromel-Alumel thermocouple connected to a digital micro voltmeter (Model: 197A, Keithley Instruments, USA).

CHAPTER 4

RESULTS AND DISCUSSION

4.1 Introduction

The results obtained from various experimental investigations performed on as-deposited PPDACH thin films are represented and discussed in this chapter. The surface morphology, chemical structure, optical and thermal properties of PPDACH thin films were investigated by means of FESEM, AFM, FTIR, UV-Vis spectroscopy and DTA/TGA, respectively. The DC electrical conduction mechanism of PPDACH thin films are also studied by DC electrical measurements.

4.2 Surface Morphology and Compositional Analyses

4.2.1 FESEM study

Figures 4.1 and 4.2 demonstrate the top view of FESEM micrographs of as-deposited PPDACH (AC) thin films of thickness 130 nm and 245 nm prepared by AC plasma taken at different magnifications (×30k, ×50k, ×100k), respectively. Surface of the PPDACH (AC) films are smooth, uniform and pinhole free as observed from the SEM micrographs, however, showing agglomerates/mosaic structure at higher magnification. It is also observed that the mosaic-like structure becomes more noticeable in the films of higher thickness. It can be visualized that during the growth of the thin films some aggregations/clusters may be formed owing to interaction among the molecular chains. This type of structure also observed by Banu et al. [63] and Nasrin et al. [64] in plasma polymerized diethanolamine and N-benzylaniline thin films prepared by AC plasma polymerization technique, respectively. Throughout the FESEM images, a few small white spots were observed at lower magnification, which is because, in some cases higher amount of monomer may be injected inside the reactor, condensed and deposited as droplet on the surface of the films. The cross sectional view of as-deposited PPDACH (AC) thin film of thickness 256 nm is shown in Fig. 4.3. In the cross sectional view of the PPDACH (AC) thin films it is also evident that the thin films contain very small grains.
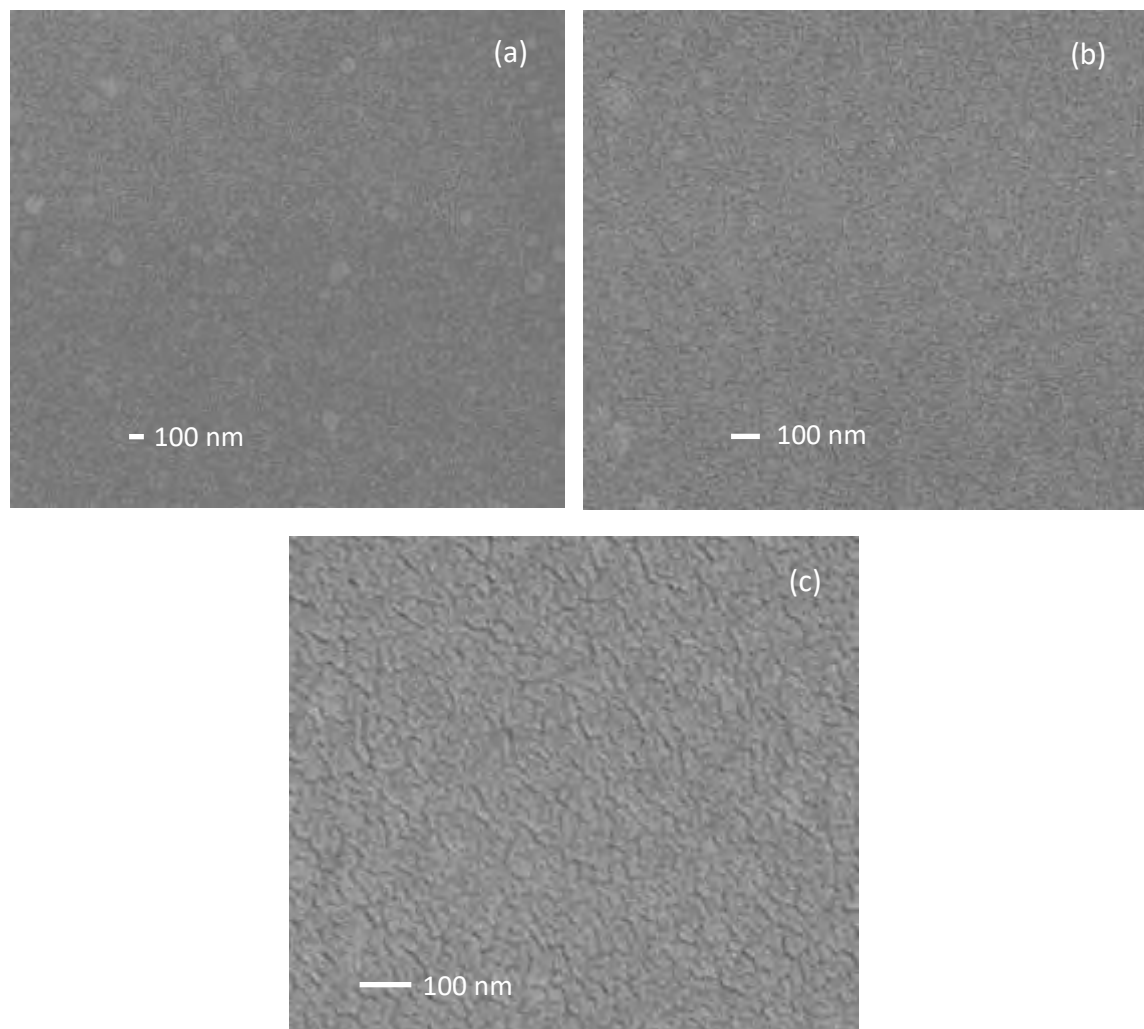
Fig. 4.1 FESEM micrographs of as-deposited PPDACH (AC) thin films of thickness 130 nm at magnifications (a) × 30 k, (b) × 50 k and (c) ×100 k.
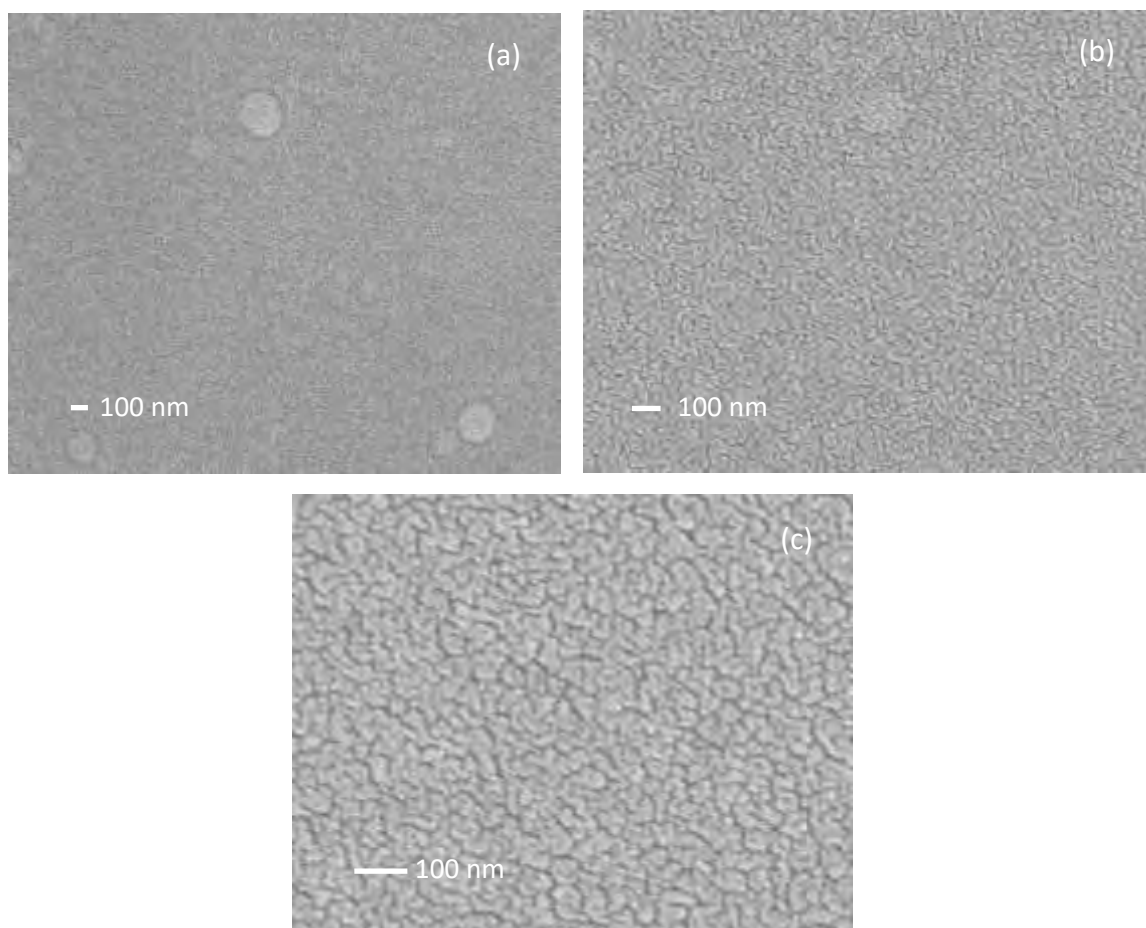
Fig. 4.2 FESEM micrographs of as-deposited PPDACH (AC) thin films of thickness 250 nm at magnifications (a) $\times$ 30 k, (b) $\times$ 50 k and (c) $\times$100 k.
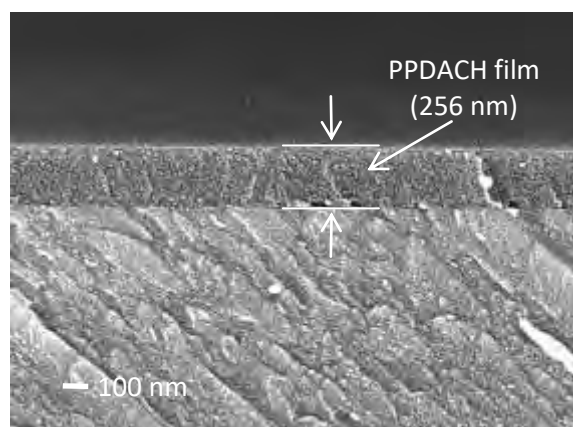
Fig. 4.3 FESEM micrograph (cross-section) of as-deposited PPDACH (AC) thin films of thickness 250 nm at magnification $\times$ 50 k.

The FESEM micrographs of the as-deposited PPDACH (RF) thin films of thicknesses 65 nm and 80 nm, prepared by RF plasma with magnifications ×30 k, ×50 k, ×100 k, are shown in Fig. 4.4 and Fig. 4.5, respectively. It is seen that the surfaces of the films are pinhole free and smooth at all magnifications. Input power influences the degree of polymerization. At higher input power, the degree of polymerization is high. RF plasma with a higher power level would cause an intense precursor fragmentation and greater effect of plasma irradiation on the polymerized surface resulting the formation of a highly smooth and uniform surface as compared to the surface of AC plasma polymerized thin films.
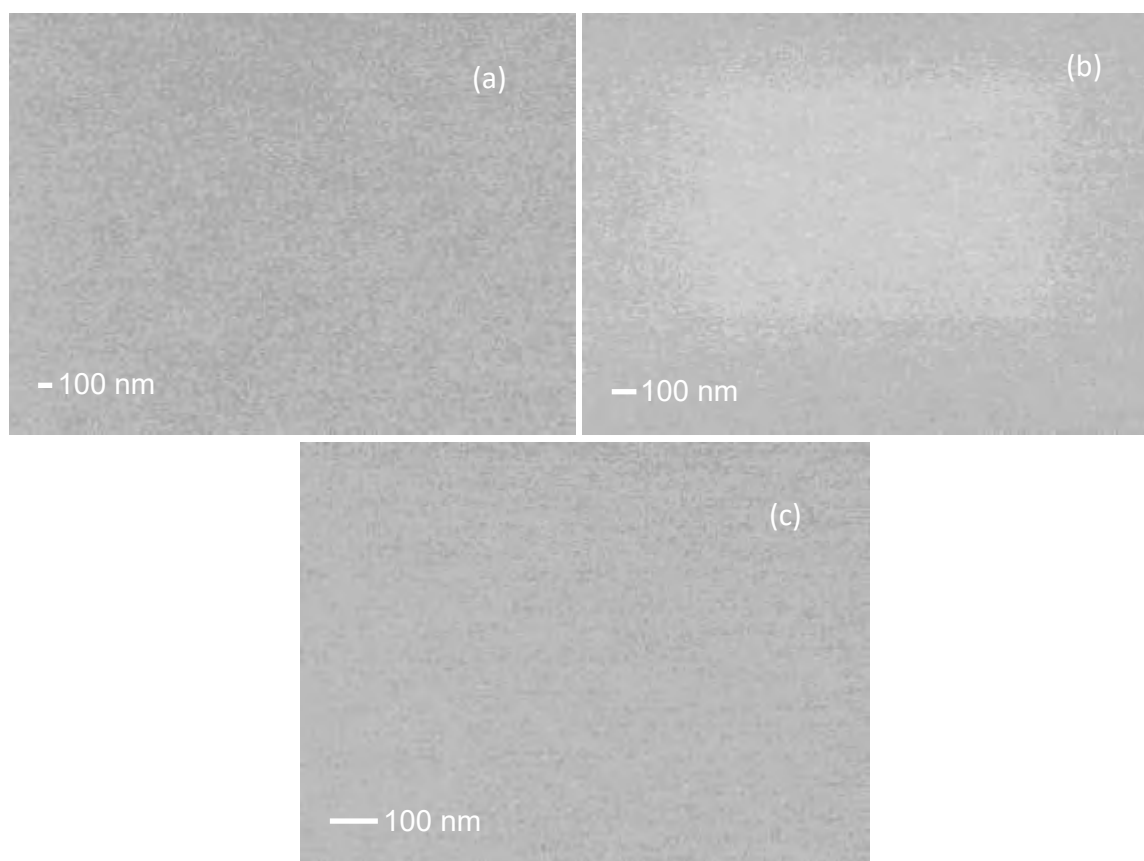
Fig. 4.4: FESEM micrograph of as-deposited PPDACH (RF) thin films of thickness 65 nm at magnifications (a) × 30 k, (b) × 50 k and (c) ×100 k.
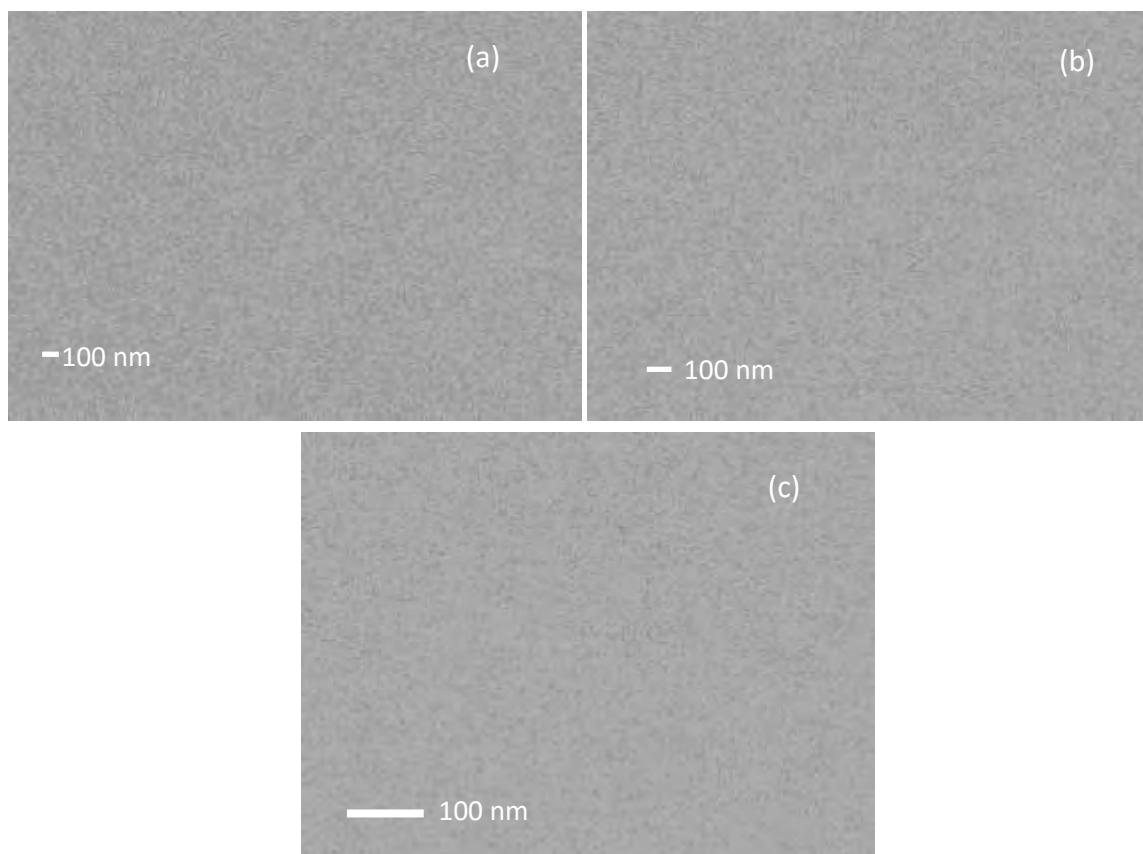
Fig. 4.5: FESEM micrographs of as-deposited PPDACH (RF) thin films of thickness 80 nm at magnifications (a) × 30 k, (b) × 50 k and (c) ×100 k.

4.2.2 Atomic force microscopy

The AFM images taken on 1 μm × 1 μm area of the samples is presented in Fig 4.8 to observe surface topography of the thin films fabricated by AC and RF plasma polymerization techniques. Figs. 4.6 (a, b) and Figs 4.6 (c, d) show AFM images of PPDACH (AC) and PPDACH (RF) thin films, respectively. Smooth, defect-free and homogeneous surface is observed which indicates the proper formation of films during polymerization. The surface morphological parameters (R_{avg}, R_{rms}, R_{sk} and R_{ku}) obtained from AFM micrographs are listed in Table 4.1. The R_{avg} and R_{rms} values are found to be very small for both PPDACH (AC) and PPDACH (RF) thin films, however, AC thin films have higher values than those of RF thin films which indicates that surface of the PPDACH (AC) films' is rougher than PPDACH (RF) thin films. Furthermore, the values

of statistical parameters R_{sk} and R_{ku} of the films are observed to be 0.49 and 5.18 for PPDACH (AC) thin films and −0.24 and 3.41 for PPDACH (RF) thin films, respectively. As the value of R_{ku} (for AC) is much more than 3.0, it indicates that the film has more peaks then the valleys as shown in the 3D image in Fig. 4.6 (b). Also the positive value of R_{sk} proposes more tops than valleys in the asymmetrical form of the film surface [65-66]. The negative value of R_{sk} for PPDACH (RF) thin films indicates that the surface is more planer and valleys are predominant [66].
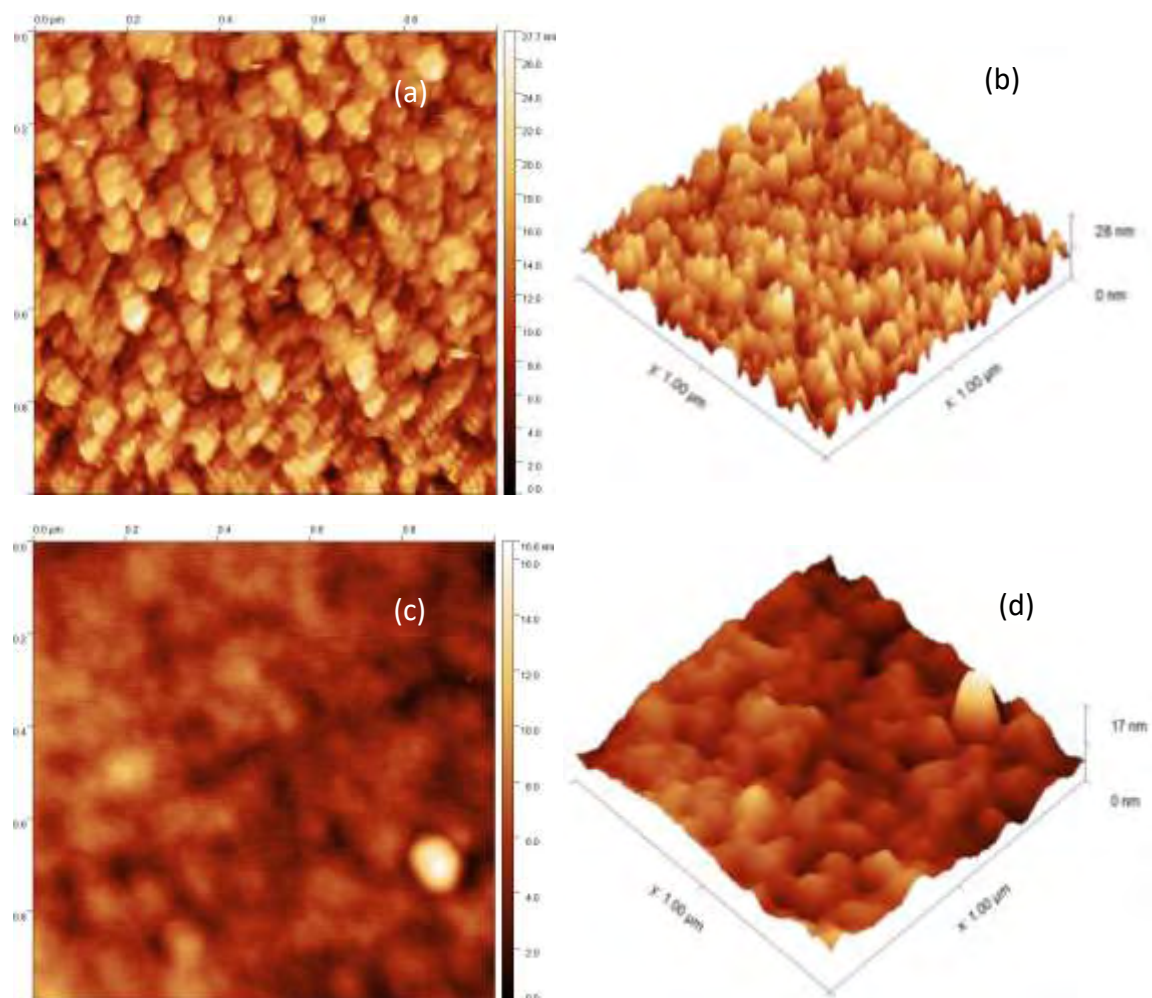
Fig 4.6: AFM micrographs (1 μm × 1 μm) of the AC plasma polymerized thin films of thickness 250 nm (a) 2D, (b) 3D view and those of RF plasma polymerized thin films of thickness 65 nm (c) 2D, (d) 3D view.

Higher RF excitation frequency provides efficient fragmentation and dissociation of the precursor gas, which forms plasma consisting of high ion flux. More surface bombardment and etching are caused by high energy RF ions which might lead to a decrease in roughness. Therefore, it can be concluded that the surface roughness of PPDACH (RF) thin films is smoother and more uniform than PPDACH (AC) thin films.

Table 4.1: Surface properties of plasma polymerized thin films obtained by AFM.

Topographical parameters	PPDACH (AC)	PPDACH (RF)
Average roughness (R_{avg})	0.89 nm	0.11 nm
Root mean square roughness (R_{rms})	1.21 nm	0.14 nm
Skewness (R_{sk})	0.49	−0.24
Kurtosis (R_{ku})	5.18	3.41

4.2.3 EDX analyses

The compositional analysis of the PPDACH thin films were performed by EDX attached to the FESEM. The EDX spectra of as-deposited PPDACH thin films are represented in Fig. 4.7 and Fig. 4.8 for the films fabricated by AC and RF plasma polymerization techniques, respectively. The atomic percentage (at%) of constituent elements of PPDACH thin films are listed in Table 4.2. The constituent elements of the monomer precursor (DACH) is also calculated and it is found that the monomer contains about 22 at% of carbon (C), 26 at% of hydrogen (H) and 52 at% of nitrogen (N).
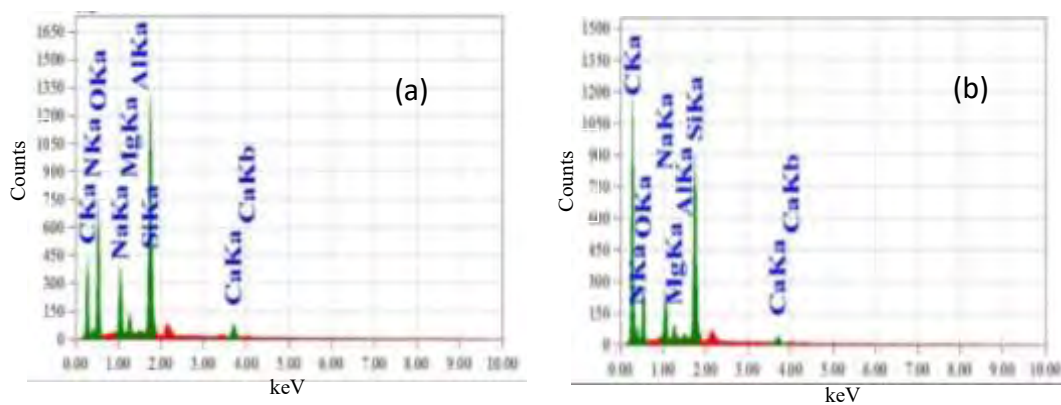
Fig. 4.7: EDX spectra of the PPDACH (AC) thin films of thicknesses (a) 130 nm and (b) 250 nm.
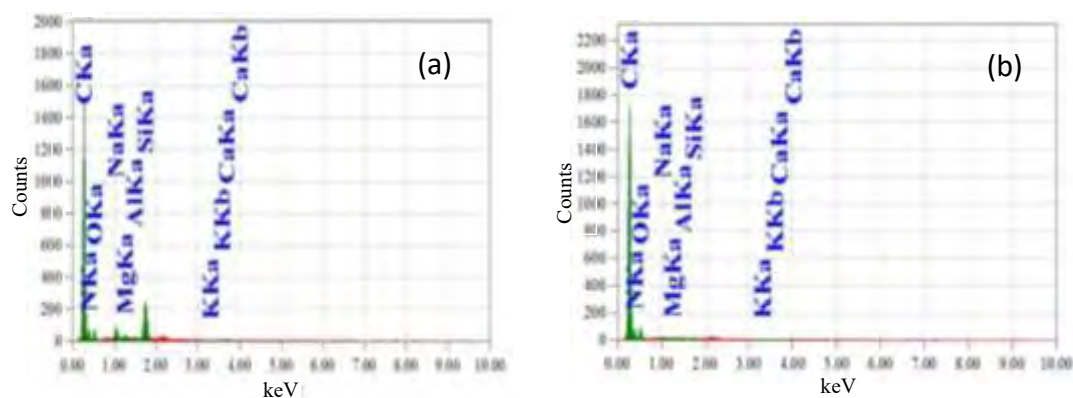
Fig. 4.8: EDX spectra of the PPDACH (RF) thin films of thicknesses (a) 65 nm and (b) 80 nm.

Table 4.2: Atomic percentage (at%) of the elements present in the DACH monomer and PPDACH thin films.

Element detected	DACH (at %) (calculated)	Elements in PPDACH (at %)			
		AC sample		RF sample	
		130 nm	250 nm	65 nm	80 nm
C	22.22	42.58	63.44	72.52	72.79
N	51.85	07.28	15.22	19.75	21.07
O	-	31.48	12.33	04.53	05.88
H	25.93	Not detected	Not detected	Not detected	Not detected
Na	-	03.54	01.84	0.65	0.07
Mg	-	01.13	00.50	0.19	0.02
Al	-	00.13	00.11	0.06	0.02
Si	-	12.12	06.03	2.19	0.11
Ca	-	01.74	00.54	0.12	0.05
Total	100.00	100.00	100.00	100.00	100.00

The at% of C and N in the PPDACH thin films are observed to increase with the increase of film thickness for both AC and RF plasma polymer, which may be caused by the probable loss of hydrogen throughout the time of plasma polymerization. In addition

to the basic components of the monomer, the polymer contains Na, Mg, Si, Ca in the PPDACH thin films, which are the elements of the substrates and are confirmed due to the decease of these elements in the EDX data with the increase in films thickness as shown in Table 4.2. The incorporation of oxygen (O) in the films may be arisen during the plasma polymerization or from atmosphere when the samples were taken out from the reactor chamber.

4.3 Structural Analyses

4.3.1 FTIR spectroscopy

The FTIR measurements have been performed to get an insight into the chemical structures of deposited thin films. It is one of the powerful tools for identifying and investigating the presence of various functional groups in polymers [67,68]. Fig. 4.9 represents the recorded FTIR spectra of the monomer and as-deposited PPDACH at room temperature in transmittance mode ranging from 4000 to 400 cm^{-1} wavenumber. The principal vibrational absorption peaks in the spectra and their tentative assignments are presented in Table 4.3.

In the spectrum of the monomer (DACH), the doublet peaks at about 3355 cm^{-1} and 3280 cm^{-1} indicate N-H asymmetric and symmetric stretching of primary amine (RNH_2), respectively [68,69]. However, in the case of PPDACH thin films the NH_2 doublet peaks are replaced by a broad peak found at about 3326 cm^{-1} and 3320 cm^{-1} in AC and RF plasma polymers, respectively which may be derived from a primary amine, a secondary amine or an imine group [68], thus confirming the formation of secondary amino group (N–H) during the plasma polymerization.

The absorption peaks observed at 2920 cm^{-1} and 2850 cm^{-1} in the spectra DACH appear due to the asymmetric and symmetric stretching vibrations of aliphatic C–H groups, respectively, which were also detected in the spectra of the PPDACH, but shifted very slightly towards higher wavenumber.

Fig. 4.9: FTIR spectra of DACH monomer; as-deposited PPDACH (AC) and PPDACH (RF) thin films of thicknesses 130 nm and 80 nm, respectively.

Two new bands at about 2355 cm^{-1} and 2210 cm^{-1} in PPDACH(AC) spectrum and at about 2360 cm^{-1} and 2190 cm^{-1} in PPDACH(RF) spectrum were developed in the plasma polymerized films which correspond to C≡C and C≡N stretching vibrations, respectively [70] and suggests decomposition of the NH$_2$ groups during the plasma process.

The peaks arise around 1630 cm^{-1} and 1625 cm^{-1} in the PPDACH spectra indicate the presence of conjugation i.e., C=C stretching vibrations. Some of the absorption peaks in the monomer such as the band at 1585 cm^{-1} for N-H vibration, ~1450 cm^{-1} and 1370

cm^{-1} for asymmetric and symmetric C–H bending vibrations, at 1245 cm^{-1} corresponding to the C–N stretching vibrations, the sharp absorption peak at about 835 cm^{-1} which is attributed to N–H wagging vibration disappear in the PPDACH spectra. These clearly suggest that the chemical structure is modified/changed during the plasma polymerization.

Table 4.3: The FTIR spectroscopic assignments for the DACH monomer, PPDACH (AC) and PPDACH (RF) thin films.

Assignment	Wavenumber (cm^{-1})		
	Monomer	PPDACH thin films	
	DACH	PPDACH (AC)	PPDACH (RF)
N–H stretch.	3355, 3280	3375	3365
C–H asym. stretch.	2920	2925	2930
C–H sym. stretch.	2850	2855	2860
$C \equiv C$ stretching	------	2355	2360
$C \equiv N$ stretching	------	2210	2190
C = C	------	1630	1650
N–H bending	1585	------	-------
C–H asym. bending	1450	------	1455
C–H sym. bend	1370	1390	1385
C–N stretch	1245	------	1125
N–H wagging	950, 835	------	------
C–H out of plane bending	635	670	675

The absorption band at 635 cm^{-1} associated with C–H out of plane bending is shifted to higher wavenumber ~ 670 cm^{-1} and ~ 675 cm^{-1} in PPDACH (AC) and PPDACH (RF) spectrum, respectively, clearly indicating the conjugation in the chemical structure [71]. Finally, it can be inferred that during the plasma polymerization primary amine (RNH_2) groups are converted into secondary amine (R_2NH) when AC or RF power is applied to the monomer. Moreover, intensity of the absorbing bands in the spectra of PPDACH has

decreased significantly as compared with those of the monomer suggesting the degradation or reorganization of the monomer molecules during the plasma polymerization.

4.3.2 XRD analysis

The XRD patterns of AC and RF plasma polymerized DACH thin films are presented in the Fig. 4.10. It is evident from the figure that there is no well-defined peak is observed except a wide hump between 2θ values of 15° and 40° indicating that the structure of the PPDACH thin films is amorphous in nature.

Fig. 4.10: The XRD patterns for AC and RF plasma polymerized DACH thin films.

4.4 UV-Visible Spectroscopic Analyses

4.4.1 AC plasma polymerized DACH thin films

Optical properties of the PPDACH thin films are studied from the UV-Vis spectra in the wavelength range of 200 nm – 800 nm at room temperature. The variation of absorbance, A, of the PPDACH thin films of different thickness with λ is shown in Fig. 4.11 (a). It is clear that the value of A rises sharply in the UV region and reaches to a maximum value at about wavelength 300 nm and then decreases rapidly up to about 450 nm for all the PPDACH thin films. After that the value of A decreases very slowly and

become almost constant at about 550 nm. The absorption peaks for all the PPDACH thin films are in the UV region and the wavelength values (λ_{max}) for the peak absorbance shifted slightly to the lower wavelength as mentioned in Table 4.4. This may be attributed to the existence of conjugation in thin film [72]. In addition, the peak values of the value of A rises with the increase of film thickness, which may be due to either increase of the carbon contents or an increase in scattering with increasing thickness.

(a)   (b)

Fig. 4.11: Spectral distribution of (a) absorbance and (b) transmittance T (%) at different thicknesses of PPDACH (AC) thin films as a function of wavelength.

Fig. 4.11 (b) represents the optical transmittance, T (%), of the PPDACH thin films of various thicknesses and indicates that T (%) increases promptly with increasing wavelength at lower range ($\sim$ 350 −550 nm) and finally reaches to almost a constant value at higher wavelengths ($\sim$ 550 − 800 nm). Thus the films can be considered to be highly transparent in the visible region. However, transmittance declines with rising thickness indicating high cross-linked density [37].

Absorption co-efficient (α) was estimated from absorbance data using equation (2.8) [73] given below and represents in Fig. 4.15.

$$\alpha = \frac{2.303\,A}{d} \qquad\qquad (4.1)$$

where, $A = log_{10}\left(\frac{I_0}{I}\right)$ with I_0 is the incident intensity and I is the transmitted intensity, and d is the path length of the absorbing species. The greater the absorption rate, the less amount of light will reach into a substrate prior to absorption. It is evident from Fig. 4.12 that the absorption edges follow an exponential fall in the low energy region, which is caused by the lack of a long range order or existence of defects in the films [74]. Furthermore, these curves are analyzed by two different slopes indicating the presence of both direct and indirect optical transitions in the PPDACH thin films.

Fig. 4.12: Plot of absorption coefficient, α with $h\nu$, for as-deposited PPDACH (AC) thin films of different thicknesses.

Optical band gap, E_{opt}, is one of the most significant optical parameters related to the electronic structure of the thin films. In order to evaluate the allowed direct and indirect optical band gaps, $E_{g(d)}$ and $E_{g(i)}$, respectively of the PPDACH thin films, the well-known Tauc relation is used [75,76], which is of the form;

$$\alpha h\nu = B\ (h\nu - E_{opt})^n \qquad (4.2)$$

Here, B is the proportionality factor, called Tauc parameter and the index n is connected with the optical transition. The index $n = 1/2$ and 2 correspond to the $E_{g(d)}$ and $E_{g(i)}$, respectively and therefore, can be estimated from the intercept of the linear portion of the curves $(\alpha h\nu)^2$ versus $h\nu$ and $(\alpha h\nu)^{1/2}$ versus $h\nu$, respectively as shown in Figs. 4.13

(a) and 4.13 (b), respectively. The estimated values of $E_{g(d)}$ and $E_{g(i)}$ of the PPDACH (AC) thin films are figured out in Table 4.4.
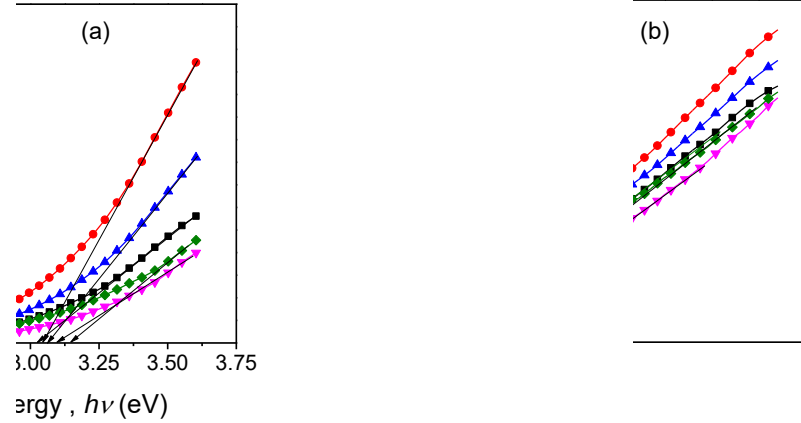
Fig. 4.13: Variation of (a) $(\alpha h \nu)^2$ and (b) $(\alpha h \nu)^{1/2}$ with $h\nu$ of PPDACH (AC) thin films of different thicknesses.

Table 4.4: Band gap and λ_{max} values of PPDACH (AC) thin films of different thicknesses.

Deposition time (min)	Thickness, d (nm)	λ_{max} (nm)	$E_{g(d)}$ (eV)	$E_{g(i)}$ (eV)
30	130	338	3.02	1.81
60	185	330	3.04	1.86
90	250	329	3.07	1.79
120	270	304	3.10	1.93
150	375	304	3.15	1.89

From Table 4.4, it is seen that $E_{g(d)}$ increases slightly with increasing thickness because some crosslinking may be developed within the bulk of the material as a result of the impact of plasma on the surface during deposition process. However, $E_{g(i)}$ values does are about 1.80 eV, which is almost independent of the film thickness.

Though, using Tauc relation and absorbance data, two types of band gaps are observed in PPDACH thin films, however, more research is required to determine which type of optical transition is active in the as-deposited PPDACH thin film and whether the films

are radiative or non-radiative. For example, photoluminescence (PL) spectroscopy of the films can be done to understand whether the material is radiative or not.

Another optical parameter, which is known as Urbach energy, represents the defect states in the optical band gap region. These localized defect states in the band gap region are responsible for the formation of absorption tail in the absorption spectra, which is known as Urbach tail and energy associated with it is called Urbach energy (E_u). In the low photon energy region, the Urbach empirical rule that describes spectral dependence of α on $h\nu$ is given by the following equation [72],

$$\alpha = \alpha_0 \exp\left(\frac{E}{E_u}\right) \qquad (4.3)$$

where, α_0 is a constant, E is the energy of incident photon. Using the logarithm on both sides of the equation (4.3), a straight line equation can be obtained.

$$\ln \alpha = ln\alpha_0 + \frac{E}{E_u} \qquad (4.4)$$

Therefore, the inverse gradients of the graphs lnα versus $h\nu$ plots as shown in Fig. 4.14 for the as-deposited PPDACH thin films of different thicknesses provide the values of E_u. The obtained E_u values have been noted in Table 4.5 and it is observed that E_u values increase with increasing film thickness, which might be occurred due to the increase of disorder in the films [33] and also suggests the introduction of localized states within the forbidden energy bandgap.
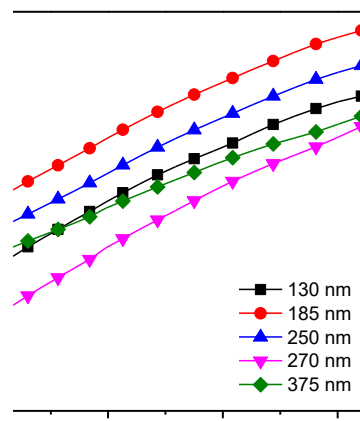
Fig. 4.14: The lnα vs $h\nu$ plots for all as deposited PPDACH (AC) thin films of various thicknesses.

Table 4.5: Variation of E_u and σ_s of as-deposited PPDACH (AC) thin films with film thicknesses.

Thickness, d (nm)	Urbach energy, E_u (eV)	Steepness parameter, σ_s
130	0.63	0.041
185	0.69	0.037
250	0.71	0.036
270	0.67	0.039
375	0.87	0.030

To study the broadening of the optical absorption edge in consequence of electron-phonon or exciton-phonon interactions, the steepness parameter, σ_s, can be estimated using the relation [63],

$$\sigma_s = \frac{k_B T}{E_u} \qquad (4.5)$$

where, k_B is the Boltzmann constant and T is the absolute temperature. The σ_s values are determined by taking $T = 298$ K and are listed in Table 4.5 and it is seen that σ_s values decreases with film thickness.

The extinction coefficient (k) is also another important optical parameter associated with the absorption. k describes the attenuation of light in a medium which can be calculated from α with the assistance of the relation,

$$k = \frac{\alpha \lambda}{4\pi} \qquad (4.6)$$

The variation k with λ for the PPDACH thin films of various thicknesses is shown in Fig. 4.15 and it is observed that k value decreases with the increase of λ indicating the possibility of decrease in electron transfer across the mobility gap with λ.

Fig. 4.15: The variation of extinction coefficient, k with λ for as-deposited PPDACH (AC) thin films of various thicknesses.

To measure how light propagates through a material refractive index, μ, can be used. The higher value of μ indicates slower velocity of electromagnetic wave through the materials. With the help of Fresnel's formula (Eq. 4.5), the values of refractive indices are measured [73] and the variation of μ against wavelength λ is plotted in Fig. 4.16.

$$\mu = \left(\frac{1+R}{1-R}\right) + \sqrt{\frac{4R}{(1-R)^2} - k^2} \qquad (4.7)$$

Fig. 4.16: The variation of μ with λ for all as-deposited PPDACH (AC) thin films.

It is pointed out that the μ values drop sharply in the lower wavelength region (350 – 600 nm). Thereafter, it becomes almost stable for all the PPDACH (AC) thin films, however, the maxima in the μ values is shifted from 340 nm to 470 nm with the increase in film thickness. Nevertheless, μ values also increase with increasing film thickness, indicating the increase in interactions taking place between the photons and electrons of the films.

On the other hand, the optical response of the deposited films can be understood with the help of optical conductivity (σ_{opt}). The variation of σ_{opt} with wavelength for different thicknesses of the films can be calculated by using the following equation [77],

$$\sigma_{opt} = \frac{\alpha n c}{4\pi} \qquad (4.8)$$

Where, c is the velocity of light. The changes in σ_{opt} are plotted against λ and are presented in Fig. 4.17 (a). It is clearly seen that σ_{opt} decreases with increasing film thickness and the maximum values of σ_{opt} decreases with the increase in film thickness. It is also noted that the value of σ_{opt} approaches zero at higher wavelengths (above 600 nm) for all the deposited thin films.

The scale of the skin depth determines the essence of the contact between an incident wave of light and the electrons in the material. Skin depth (χ) is defined as the depth at which the electromagnetic wave will have its amplitude reduced by a factor 1/e. The skin depth, χ is to be obtained by the relation [78],

$$\chi = \frac{\lambda}{2\pi k} \qquad (4.9)$$

The dependence of skin depth on energy is demonstrated in Fig. 4.17 (b). It is observed that χ decreases monotonically with increasing photon energy and slightly changes with the thicknesses of the films. The skin depth is reduced at a higher energy range due to the energy loss because of increase in collisions of electrons.
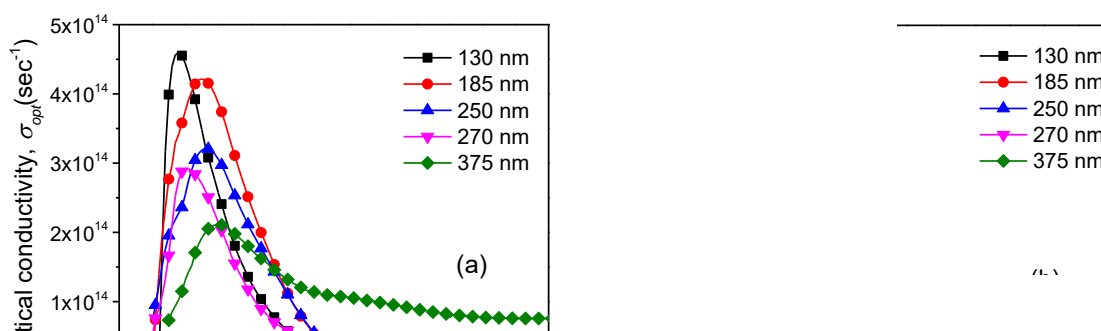
Fig. 4.17: (a) The plots of optical conductivity (σ_{opt}) against λ and (b) The variation of skin depth (χ) with photon energy for PPDACH (AC) thin films of different thicknesses.

4.4.2 RF plasma polymerized DACH thin films

The variation of A and T (%) with λ for the PPDACH (RF) thin films of different thicknesses obtained by RF plasma polymerization technique are shown in Fig. 4.18. It is seen that the absorption peak intensity does not changed significantly. The λ_{max} and A_{max} values corresponding to the thickness of the PPDACH (RF) thin films are recorded in Table 4.6. Above 500 nm, absorbance becomes almost zero which suggests that the films are transparent in this region.

Fig. 4.18: Spectral distribution of (a) absorbance and (b) transmittance T (%) for different thicknesses of PPDACH (RF) thin films as a function of wavelength.

The absorption co-efficient α have been calculated from the absorbance data and the spectral dependence of α as a function of energy $h\nu$ is shown in Fig. 4.19. It is observed that the thin films of lower thickness have higher values of the absorption coefficients at higher energies, which indicates that in the films of lower thickness the intensity of light is reduced more.

Fig. 4.19: The dependence of α with $h\nu$ for PPDACH (RF) thin films of different thicknesses.

It is clear that the curves have different slopes indicating the presence of several optical transitions in the PPDACH (RF) thin films. The $(\alpha h\nu)^2$ vs $h\nu$ and $(\alpha h\nu)^{1/2}$ vs $h\nu$ for PPDACH (RF) thin films of different thicknesses are plotted in Fig. 4.20.
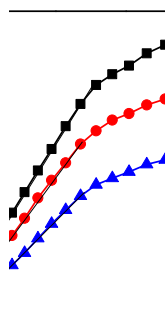
Fig. 4.20: (a) $(\alpha h\nu)^2$ vs $h\nu$ and (b) $(\alpha h\nu)^{1/2}$ versus $h\nu$ curves for PPDACH (RF) thin films of different thicknesses.

Both the direct, $E_{g(d)}$ and indirect, $E_{g(i)}$ energy gaps are determined from the intercept of the extrapolation of the curves to zero α in the photon energy axis. The values $E_{g(d)}$ and $E_{g(i)}$ are documented in Table 4.6. The $E_{g(d)}$ values $_{are}$ nearly equal (~4.04 eV) whereas $E_{g(i)}$ decreases from 2.78 -2.58 eV with increasing thickness of the films.

Table 4.6: Maximum wavelength (λ_{max}) corresponding to maximum absorbance (A_{max}) and the variation of band gaps with thickness (d).

Thickness, d (nm)	λ_{max} (nm)	A_{max}	$E_{g(d)}$ (eV)	$E_{g(i)}$ (eV)
66	232	1.66	4.04	2.78
70	231	1.62	4.03	2.62
80	233	1.66	4.01	2.58

The plots of $ln\alpha$ vs $h\nu$ for all as-deposited PPDACH (RF) thin films are presented in Fig. 4.21 and the inverse gradient of these graphs provides the values of Urbach energy, E_u. The obtained E_u values have been recorded in Table 4.7. It is observed that E_u values decrease with increasing film thickness which might be occurred due to the structural defects. This is an evidence for the decrement of defect levels. The steepness parameter, σ_s, can be estimated using the equation (4.5) and are listed in Table 4.7. It is seen that the σ_s increases with increasing thicknesses of the films.

Fig. 4.21: The $ln\alpha$ vs $h\nu$ plots for different thicknesses of as deposited PPDACH (RF) thin films.

Table 4.7: Variation of E_u and σ_s for as-deposited PPDACH (RF) thin films with film thicknesses.

Thickness, d (nm)	Urbach energy, E_u (eV)	Steepness parameter, σ_s
65	0.96	0.027
70	0.65	0.040
80	0.52	0.050

The extinction coefficient, k, can be calculated with the help of the relation (4.6), The variation of k with λ for various thicknesses of the PPDACH (RF) thin films are shown in Fig. 4.22 (a). The peaks are found in the UV region near the wavelength 250 nm and observed that the k values are lower for thin films of higher thickness. The k values also decrease with the increase of λ and become almost zero above 500 nm indicating that films are transparent in the visible region. Refractive index of the PPDACH (RF) thin films is calculated by the equation (4.7) and plotted against λ in Fig. 4.22 (b).

Fig. 4.22: Variation of (a) extinction coefficient (k) and (b) refractive index with wavelength (λ) for PPDACH (RF) thin films of different thicknesses.

The value of μ continues to increase with increasing wavelength, λ up to 375 nm and then decreases up to 500 nm. After that it becomes constant in the visible region.

Therefore, it can be said that light moves faster through the films in the visible region and those exhibits higher transmittance.

The values of σ_{opt} of the films was calculated using the Eq. (4.8) and are plotted against λ, which is shown in Fig. 4.23 (a). It is observed that σ_{opt} changes rapidly till to the wavelength, 500 nm and then it becomes steady. At lower wavelength region, σ_{opt} is maximum, that is, the absorbance is highest. The χ values for as deposited PPDACH (RF) thin films are estimated using the relation (4.9). Fig. 4.23 (b) depicts the dependence of χ on E. From this figure, it is seen that χ is large at low energy region whereas at high energy region it shows lower value.
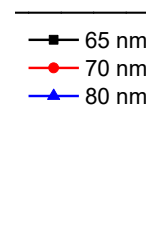
Fig. 4.23: (a) The variation of σ_{opt} with λ and (b) The variation of χ with photon energy for as deposited PPDACH (RF) thin films of different thicknesses.

4.5 Thermal Analyses

The TGA and DTA have been carried out to characterize the decomposition and the thermal stability of the PPDACH thin films. The TGA and DTA traces taken for AC and RF plasma polymer at heating rate of 20 °C/min in nitrogen atmosphere in the temperature range of 25 – 1000 °C.

4.5.1 TG/DTA of AC plasma polymerized DACH films

Fig. 4.24 depicts the DTA and TGA curves for AC plasma polymerized DACH powder samples in N_2 environment. The TGA trace of PPDACH (AC) has revealed different stages of mass loss due to heating. The weight losses in A, B and C regions are about 5%, 3% and 63% respectively and 29% remains.

Fig.4.24: The TGA and DTA thermograms of PPDACH (AC) thin films in N_2 environment at scanning rate of 20 °C /min.

In the low temperature region (A) i.e. up to about 100 °C, the weight loss may be due to the elimination of absorbed surface water or which is not necessarily associated with any change in the PPDACH structure. After that, there is a plateau region (B) up to 282 °C where weight loss is small near about 3%. And in region C, after temperature 282 °C a huge weight loss is observed which may be due to the thermal decomposition or breakdown reaction. DTA trace in region C shows a wide exothermic peak at the temperature 390 °C indicating a gradual change of its original properties. Thus, it can be inferred that the PPDACH is thermally stable up to about 282 °C in N_2 atmosphere.

4.5.2 TG/DTA of RF plasma polymerized DACH films

The TG/DTA traces taken at 20 °C/min for RF plasma polymerized DACH powder samples in N_2 atmosphere are shown in Fig. 4.25.

15

— TGA   10
— DTA

5

0

-5
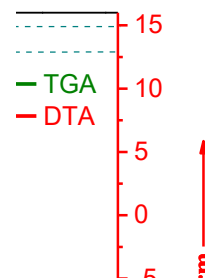
Fig. 4.25: The TGA and DTA thermograms of PPDACH (RF) thin films in N_2 environment at scanning rate of 20 °C /min.

The TGA trace of PPDACH thin films has been taken from 25 to 1000 °C and showed different stages of thermal decomposition owing to heating, which divided in three regions (A, B, and C). Every region may be associated with a different rate of weight loss. The weight losses in A, B and C regions are about 3%, 1% and 38%, respectively and 58% remains. In region A i.e., up to about 90 °C, the weight loss may be due to the loss of absorbed moisture in the PPDACH films. After that, there is a plateau region (B) up to 165 °C where mass loss is small near about 1% and then mass decreases. Though no significant weight loss is observed in region A and B, but the weight losses significantly at C region is about 38%. Mass losses observed from 165 °C to 930 °C which results from polymer decomposition/ breakdown. reaction might have occurred due to the evolution of low molecular weight hydrocarbon compounds. The DTA thermogram shows an exothermic broad band, which reaches a maximum at around

390 °C indicating that the rate of mass loss becomes faster. Thus, it may be attributed that PPDACH films are thermally stable up to about 165 °C.

4.5.3 Comparison of thermal behavior between AC and RF plasma thin films

The TGA curves for PPDACH films in N_2 environments are shown in Fig. 4.26.

Fig. 4.26: Comparison of weight loss of PPDACH thin films in nitrogen atmosphere.

For PPDACH (AC), the weight losses, which actually occur due to heating, in A, B and C regions are 5%, 3%, and 65 %, respectively and remaining weight is 27 % whereas for PPDACH (RF), the weight losses in A, B and C regions are 3 %, 1%, and 40%, respectively and remaining weight is 56%. It is observed from Fig. 4.13 that the AC plasma polymerized thin film is thermally stable up to about 280 °C, whereas RF plasma polymerized thin film is stable up to about 165 °C, however the decomposition is delayed for the PPDACH (RF) thin films.

4.6 DC Electrical Properties of Plasma Polymerized PPDACH (AC) Thin Films

Various carrier transport mechanisms in insulating polymer thin films based on the dependence of current density (J) on voltage (V), temperature (T), and thickness (d) have been suggested. In order to determine the predominance of a certain mechanism, the dependency of the current density on the described parameters needs to been analyzed.

4.6.1 Current density-voltage (*J-V*) characteristics

A typical *J-V* characteristic for PPDACH (AC) thin films of thickness 135, 180 and 250 nm were recorded at various temperatures in the voltage range of 0.3 V to 100 V, and are shown in Fig. 4.27. From the figure, it is observed that the current density increases with increasing voltage and temperature. The curves have approximately same shape, having two sections of different slopes in the low and high voltage regions that imply two different conduction processes. The *J-V* characteristics follow a power law of the form $J \propto V^n$ with different values of '*n*' (slope), where *n* is a power index [79]. In the low voltage region (< 15V), the value of slopes (n) lies in between $0.10 \leq n \leq 0.44$ indicating Ohmic conduction mechanism whereas in the high voltage region (>15 V), the slope of the graph is found to lie in 1.26 – 6.01, indicating a non-Ohmic conduction mechanism. In the higher voltage region, the three main transport mechanisms typically observed in organic polymer thin films and these are Richardson–Schottky (RS) conduction, Poole–Frenkel (PF) conduction, and space-charge-limited conduction (SCLC) [80, 81]. The dependence of J on d obeys the relation $J \propto d^l$, where l is a parameter depends on the presence of traps in the films. The value of $l \geq 3$ indicates the SCLC mechanism while $l < 3$ for Schottky or PF conduction mechanism. To study the actual conduction mechanism, J is plotted against d, of different thickness of PPDACH (AC) thin films in the non-Ohmic region at 60 V which is presented in Fig. 4.28.

Fig. 4.27: *J-V* relationship for PPDACH (AC) films of thickness (a) 135 nm, (b) 180 nm and (c) 250 nm at different temperatures.

The linear slope derived from Fig. 4.28 gives a negative value of 0.75, which is much smaller than corresponding to SCLC mechanism. So, these observations do not signify the possibility of presence of SCLC mechanism in PPDACH (AC) thin films. Therefore, it may be inferred that the conduction mechanism of career transport operative in these films may either be Schottky or PF.

Table 4.8 The slopes in the lower and higher voltage regions at different temperatures for PPDACH (AC) thin films of different thicknesses.

Thickness d (nm)	Measurement temperature (K)	Value of slopes, n	
		Low voltage region ($< 15V$) (Ohmic)	High voltage region ($> 15V$) (non-Ohmic)
	298	0.27	1.37
	308	0.28	1.26
	318	0.26	1.38
135	328	0.26	1.33
	338	0.30	1.62
	348	0.37	1.57
	358	0.37	1.60
	373	0.44	1.33
	298	0.18	1.31
	308	0.16	1.49
	318	0.15	2.05
180	328	0.11	2.33
	338	0.12	2.52
	348	0.10	2.91
	358	0.05	4.09
	373	0.12	3.43
	298	0.23	6.01
	308	0.17	5.69
	318	0.13	5.69
250	328	0.16	5.67
	338	0.19	5.47
	348	0.21	5.40
	358	0.20	5.37
	373	0.36	4.71

Fig. 4.28: Plots of J vs d for PPDACH (AC) thin films in the non-Ohmic region (at voltage 60 V).

For RS or PF conduction mechanism, plot of log J vs. $V^{1/2}$ will provide a linear characteristic while for SCLC, double log plot of the form log J - log V should provide a linear characteristic. The variation of log J with log V and log J with $V^{1/2}$ for different film thicknesses are demonstrated in Figs. 4.29 (a) and (b), respectively.

Fig. 4.29: Plots of (a) log J vs log V and (b) log J vs $V^{1/2}$ of PPDACH (AC) thin films of different thicknesses.

From figure, it is observed that the plots of log J vs $V^{\frac{1}{2}}$ is more linear at higher voltage region as compared to log$J$ vs log$V$ plot suggesting the possibility that PF or RS conduction may dominate in this region.

To discern the mechanism of RS from PF, theoretical parameters (β_{PF} and β_{RS}) can be compared with experimentally determined β coefficient (β_{exp}) [82]. The experimental values of β_{exp} are evaluated by equation (2.13). The theoretical coefficients β_{S} and β_{PF} are obtained from equations (2.7) and (2.10), respectively. The values of β_{RS}, β_{PF} and β_{exp} are listed in Table 4.9.

Table 4.9: Theoretical (β_{RS} and β_{PF}) and experimental (β_{exp}) values of β coefficient coefficients for as-deposited PPDACH thin films.

Thickness, d (nm)	Temperature (K)	β coefficient (10^{-6} eV m$^{1/2}$V$^{-1/2}$)		
		β_{exp}	β_{RS}	β_{PF}
135		1.30	2.21	4.42
180	298	2.25	2.32	4.64
250		2.43	2.64	5.28

Table 4.9 shows that β_{exp} is better consistent with β_{RS} and therefore the dominant carrier transport in PPDACH (AC) thin films at higher voltage is Schottky type.

4.6.2 Dependence of J on temperature

Arrhenius law is applied to investigate the temperature dependence of the current density, J. The Arrhenius equation can be expressed as

$$J = J_0 \exp\left(-\frac{\Delta E}{k_B T}\right) \quad \ldots\ldots\ldots\ldots (4.1)$$

Where, J_0 is the current density at the thermal equilibrium, ΔE is the activation energy and k_B is the Boltzmann constant. The dependence of J on $1/T$ for PPDACH (AC) thin films of different thicknesses are shown in Fig. 4.30 (a-b). From Fig. 4.30, it is observed that each of the curves has two different slopes, one in the low temperature region (<330 K) and other in the higher temperature (> 330 K) region.

Fig. 4.30: Variation of J with $1/T$ for PPDACH (AC) thin films of thicknesses 135 nm, 180 nm and 250 nm at (a) 10 V (Ohmic) and (b) 60 V(non-Ohmic) regions.

The activation energies are evaluated in the two temperature regions at the higher ($V =$ 60 V) and lower ($V = 10$ V) voltages from the slopes of J versus $1/T$ curves and are documented in Table 4.10.

Table 4.10: Values of activation energy ΔE (eV) for PPDACH (AC) thin films of different thicknesses.

Thickness,	Activation energies, ΔE (eV)			
d (nm)	10 V		60 V	
	Temperature (K)		Temperature (K)	
	Low (<330 K)	High (> 330 K)	Low (<330 K)	High (> 330 K)
135	0.18	0.28	0.29	0.50
180	0.19	0.27	0.30	0.90
250	0.15	0.30	0.25	0.41

At an applied voltage of 10 V in the low temperature regions, the activation energies are found to be around an average value of 0.17 eV and that in the higher temperature region is about 0.28 eV, whereas, in the low and high temperature regions activation energies were found to be around an average value of 0.28 eV and 0.60 eV, respectively for an applied voltage of 60 V. In the low temperature regions, low activation energy suggests that the thermally activated hopping conduction is operational in these films. A shift from hopping regime to a regime with distinct energy levels might be linked to the change from lower to higher values in activation energy in the high temperature regions [83].

4.7 DC Electrical Properties of PPDACH (RF) Thin Films

4.7.1 *J-V* characteristics

In order to explain the DC electrical conduction mechanism in PPDACH (RF) thin films, dependence of *J* have been observed on PPDACH (RF) thin films of various thicknesses in the voltage range 0.3 to 100 V at different temperatures.

Fig. 4.31: Current density (*J*) - Voltage (*V*) relationship at different temperatures for PPDACH (RF) films of thickness (a) 65 nm, (b) 70 nm and (c) 85 nm.

The observed *J-V* characteristics of the PPDACH (RF) films of different thickness at various temperatures are presented in Fig. 4.31 (a-c). Similar to those of PPDACH (AC) films each *J–V* curve of the PPDACH (RF) films also demonstrates two different slopes in the lower and higher voltage regions which indicate two different conduction processes according to the power law with different values of *n*.

Table 4.11: The slopes in the lower and higher voltage regions at different temperature for PPDACH (RF) thin films of different thicknesses

Thickness, d (nm)	Temperature, T (K)	Value of slopes, n	
		Low voltage region (<15V) (Ohmic)	High voltage region (> 15V) (non-Ohmic)
65	298	0.24	0.81
	308	0.15	0.91
	318	0.14	1.06
	328	0.23	1.01
	338	0.34	1.24
	348	0.66	0.76
	358	0.71	0.79
	373	0.99	0.85
70	298	0.21	0.86
	308	0.15	0.89
	318	0.19	1.10
	328	0.24	1.11
	338	0.33	1.14
	348	0.50	1.19
	358	0.56	1.21
	373	0.97	1.46
85	298	0.16	1.13
	308	0.22	1.13
	318	0.25	1.31
	328	0.22	1.43
	338	0.31	1.44
	348	0.36	1.61
	358	0.42	1.76
	373	0.81	1.72

At the lower voltages region (<15 V), the values of slope $0.14 \leq n \leq 0.99$ indicate approximate Ohmic region while at the higher voltage region (>15 V), the slopes of $0.63 \leq n \leq 1.76$ represent the non-Ohmic region.

The dependence of J on d at 60 V is depicted in Fig. 4.32. The linear slope derived from Fig. 4.32 gives a negative value of 4.38, which is much higher than corresponding to RS or PF conduction mechanism. So, this observation does not signify the possibility of presence of RS or PF mechanism in PPDACH (RF) thin films. Therefore, it may have inferred that the conduction mechanism of carrier transport operative in these films is SCLC.

Fig. 4.32: Plots of J-d for PPDACH (RF) thin films in the non-Ohmic region (at 60 V).

4.7.2   Dependence of J on temperature

The variation of J with inverse absolute temperature $1/T$ for the PPDACH (RF) thin films of different thicknesses are presented in Fig. 4.33. Each of the curves is characterized by two different slopes in the low (< 330 K) and high (> 330 K) temperature regions. The activation energies calculated from the slope of J vs $1/T$ curves and the values are set out in Table 4.12.

Fig. 4.33: Variation of *J* on *1/T* for PPDACH (RF) thin films of thicknesses 65 nm, 70 nm 85 nm at (a) 10 V (Ohmic) and (b) 60 V (non-Ohmic) regions.

Table 4.12: Values of activation energy *ΔE* (eV) for PPDACH (RF) thin films of different thicknesses.

Thickness,	Activation energies, *ΔE* (eV)			
d (nm)	10 V		60 V	
	Temperature (K)		Temperature (K)	
	Low (<330 K)	High (>330 K)	Low (<330 K)	High (>330 K)
65	0.11	0.19	0.12	0.24
70	0.12	0.40	0.12	0.52
85	0.12	0.44	0.13	0.55

The activation energy in the low temperature region is almost same (~ 0.12 eV) for applied voltage 10 V and 60 V as shown in Table 4.12. On the other hand, at the higher temperature region, the activation energy is observed to increase with increasing film thickness for both applied voltage. The low and high values of activation energy in the low and high temperature region indicate the transition of carriers between defects within the band gaps and the transition of carriers between the bands, respectively.

4.8 Comparison Among Various Characteristics of PPDACH (AC) and PPDACH (RF) Thin Films

In Table 4.13, several properties of AC and RF plasma polymerized thin films such as morphological, structural, thermal, optical and conduction mechanisms acquired from various experimental investigations are recorded. It is observed that all the films obtained from both AC and RF plasma polymerization techniques show smooth, uniform and pinhole-free surfaces with amorphous structures. PPDACH (AC) films are thermally more stable (~280 ^{o}C) than PPDACH (RF) films. Schottky and SCLC type conduction mechanisms are found to be dominant in the PPDACH (AC) and PPDACH (RF) thin films, respectively.

Table 4.13 Morphological, structural, thermal, optical and DC electrical properties of as-deposited PPDACH (AC) and PPDACH (RF) thin films.

Property	PPDACH (AC)	PPDACH (RF)	Previous works
Surface morphology	Smooth and pinhole free with mosaic like structure	Smooth and pinhole free	Smooth, uniform and pinhole free [63,84]
Crystallinity	Amorphous	Amorphous	Amorphous [64, 85]
Thermal stability	Stable up to 280 ^{o}C	Stable up to 165 ^{o}C	~ 236 ^{o}C [33]
Direct band gap	3.02 – 3.15 eV	4.01 – 4.04 eV	3.18 – 3.56 eV [85], 3.64 – 3.80 eV [86]
Indirect band gap	1.79 – 1.93 eV	2.58 – 2.78 eV	1.90 – 2.22 eV [85], 3.38–3.45 eV [86]
Conduction mechanism	Richardson-Schottky (RS)	Space-charge-limited conduction (SCLC)	RS [34], SCLC [30, 24]

CHAPTER 5

SUMMARY AND CONCLUSIONS

5.1 Summary

A capacitively coupled parallel plate glow discharge plasma reactor was used to fabricate PPDACH thin films onto glass substrates. Several characterizations such as FESEM, AFM, FTIR, XRD, UV-Vis spectroscopy, TG/DTA and DC electrical measurements were carried out to investigate the morphological, structural, thermal, optical and DC electrical properties of the PPDACH thin films of different thicknesses.

Surface morphological and topographical studies of the AC and RF PPDACH thin films were carried out by FESEM and AFM analyses, respectively. All the films are found smooth, flawless and pin-hole free. However, mosaic-like structure was observed in the FESEM images of the PPDACH (AC) thin films, while very smooth surface was found for the PPDACH (RF) thin films. It is seen from the AFM studies that the roughness of the PPDACH (RF) thin films is lower than the PPDACH (AC) thin films. The EDX analysis indicates the presence of prominent percentage of C, N and a few percentage of O in PPDACH thin films, which may come from the atmosphere. The films are amorphous in nature, which is confirmed by XRD.

In order to understand the chemical structure and optical properties of the films, the FTIR and UV-Vis-spectroscopy are used, respectively. From the FTIR analyses, it is observed that the primary amine (RNH_2) converted to secondary amine (R_2NH) during the polymerization process due to the effect of both AC and RF plasma. As compared to the monomer spectrum, the intensity of absorbing bands has decreased significantly, and few new peaks are found in the plasma polymer spectra, which are not present in the monomer spectrum. These are the indication of degradation or re-organization of the monomer molecules during the plasma polymerization process.

For the PPDACH (AC) thin films, it is found that value of $E_{g(d)}$ increases from 3.02 to 3.15 eV with increasing thickness of the films. The films also have indirect band gap which remains almost constant. However, the values of $E_{g(d)}$ for the PPDACH (RF) thin films are higher (~ 4.03 eV) compared to PPDACH (AC) thin films, but remain almost independent on the film thickness.

The thermal analyses of PPDACH thin films in N_2 environment reveal that PPDACH (AC) thin films are thermally stable up to about 280 ^{o}C, whereas PPDACH (RF) films are stable up to about 165 ^{o}C. The weight loss for PPDACH (AC) thin film is greater than that of the PPDACH (RF) thin film. Thus it can be inferred that though AC plasma polymerized thin films are more stable as compared to the RF plasma polymerized thin film, however, their degradation is delayed for RF plasma films.

The J-V characteristics revealed that the dependence of J on V is Ohmic in the lower voltage region and in higher voltage region it is non-Ohmic. It is found that the dominant conduction mechanism in the PPDACH (AC) thin films is Schottky type, whereas the PPDACH (RF) thin films exhibited SCLC mechanism. The ΔE values of the PPDACH (AC) thin films in the Ohmic region are found to be 0.15 – 0.19 eV and 0.27 – 0.30 eV for lower and higher temperatures, respectively. However, in the non-Ohmic region, values of ΔE are observed to be 0.25 – 0.30 eV and 0.41 – 0.90 eV, respectively at lower (<330 K) and higher temperature (>330 K) regions. Also the values of ΔE for the PPDACH (RF) thin films in the low temperature region are found almost the same (~0.12 eV), whereas in the higher temperature region, that increased from 0.24 – 0.44 eV and 0.19 – 0.55 eV at 10 V and 60 V, respectively.

5.2 Conclusions

It is concluded that high quality of PPDACH thin films have been successfully deposited on to glass substrates by AC and RF plasma polymerization technique. RF plasma can produce PPDACH thin films of better surface morphology than AC plasma.

The structure of the monomer partially changed by forming some new bonds such as C≡C, C≡N and C=C during the polymerization, indicating a defragmentation of the monomer. The films are amorphous in nature and thermally very stable, however AC

plasma polymerized thin films are more stable as compared to the RF plasma polymerized thin films. The E_g values remained within the insulating region and therefore, these thin films can be used as insulators for the application of flexible coating on electrical devices (e.g., printed circuit board, circuit breakers, etc.).

Based on the transparency and refractive index, films can be used as anti-reflective coating in optical devices such as lenses or as encapsulant in LEDs.

The dominant conduction mechanism in the PPDACH (AC) thin films is Schottky type, whereas the PPDACH (RF) thin films exhibited SCLC mechanism.

Finally, the PPDACH thin films were found to be physically, chemically and optically stable. The outcomes of the fundamental characterizations of PPDACH thin films suggest that the material can be used as an insulating layer in electronic and optoelectronic devices.

5.3 Scope of the Further Research

In this present work, various characterizations such as morphological, structural, thermal, optical and DC electrical properties of as-deposited AC and RF plasma polymerized 1,2-diaminocyclohexne thin films are performed. Apart from this, some additional characterizations can be carried out in order to enhance the suitable applications of PPDACH thin films.

X-ray photoelectron spectroscopy (XPS) measurement can be carried out with a view to investigate the chemical composition of the PPDACH thin films.

Low temperature (< 573 K) annealing could also be performed to assess the influence of heat treatment on the electrical properties of PPDACH thin films.

Photoluminescence (PL) spectroscopy measurement can be performed to ensure the type of electronic transition (either direct or indirect) in the PPDACH thin films.

AC electrical properties of the PPDACH thin films can be done to better understand the electrical and dielectric properties of the material.

References

[1]   Patil, R. B., Jatratkar, A. A., Devan, R. S., Ma, Y., Puri, R. K., Puri, V., and Yadav, J. B., "Effect of pH on the Properties of Chemical Bath Deposited Polyaniline Thin Film," *Appl. Surf. Sci.*, vol. 327, pp. 201–204, 2015.

[2]   Yadav, J. B., Puri, R. K., and Puri, V., "Improvement in Mechanical and Optical Properties of Vapour Chopped Vacuum Evaporated PANI/PMMA Composite Thin Film," *Appl. Surf. Sci.*, vol. 254, pp. 1382–1388, 2007.

[3]   Deshmukh, P. R., Pusawale, S. N., Shinde, N. M., and Lokhande, C. D., "Growth of Polyaniline Nanofibers for Supercapacitor Applications Using Successive Ionic Layer Adsorption and Reaction (SILAR) Method," *J. Korean Phys. Soc.*, vol. 65, pp. 80–86, 2014.

[4]   Liao, C., and Gu, M., "Electroless Deposition of Polyaniline Film Via Autocatalytic Polymerization of Aniline," *Thin Solid Films*, vol. 408, pp. 37–42, 2002.

[5]   Yasuda, H., "*Plasma Polymerization,*" Academic Press, New York, 1985.

[6]   Schiller, S., Hu, J., Jenkins, A. T. A., Timmons, R. B., Sanchez-Estrada, F. S., Knoll, W., and Forch, R., "Plasma Polymerization of Maleianhydride Film Chemical Structure and Properties," *Chem. Mater.*, vol. 14, pp. 235–242, 2002.

[7]   Bae, I. S., Cho, S. H., Lee, S. B., Kim, Y., and Boo, J. H., "Growth of Plasma-Polymerized Thin Films by PECVD Method and Study on Their Surface and Optical Characteristics," *Surf. Coat. Technol.*, vol. 193, pp. 142– 146, 2005.

[8]   Cho, S. J., Bae, I. S., Jeong, H. D., and Boo, J. H., "A Study on Electrical and Mechanical Properties of Hybrid Polymer Thin Films by A Controlled TEOS Bubbling Ratio," *Appl. Surf. Sci.*, vol. 254, pp. 7817–7820, 2008.

[9]   Jiang, H., Hong, L. G., Venkatasubramanian, N., Grant, J. T., Eyink, K., Wiacek, K., Fries-Carr, S., Enlow, J., and Bunning, T. J., "The Relationship Between Chemical Structure and Dielectric Properties of Plasma-Enhanced Chemical Vapor Deposited Polymer Thin Films," *Thin Solid Film*s, vol. 515, pp. 3513–3520, 2007.

[10]   Yun, H. P., Hiroaki, T., Shigeru, T., and Seizo, M., "Electrical Properties of Plasma-Polymerized Thin Films," *Polym. J.*, vol. 18, pp. 713 – 718, 1986.

[11] Myung, S. W., and Choi, S. H., "Chemical Structure and Surface Morphology of Plasma Polymerized-Allylamine Film," *Korean J. Chem. Eng.*, vol. 23, pp. 505–511, 2006.

[12] Pachonik, H., "Production of Thin Glow-Polymerized Layers," *Thin Solid Films*, vol. 38, pp. 171–182, 1976.

[13] Tibbit, J. M., Bell, A. T., and Shen, M., "Dielectric Relaxations in Plasma Polymerized Hydrocarbons and Fluorocarbons," *J. Macromol. Sci.-Chem. A*, vol. 10, pp. 519–533, 1976.

[14] Bui, A., Carchano, H., and Sanchez, D., "Properties of Polymer Thin Films on Silicon," *Thin Solid Films*, vol. 13, pp. 207–211, 1972.

[15] Maisonneuve, M., Segui, Y., and Bui, A., "Electrical Properties of Metal-Polymer (Polysiloxane)-Silicon Structures and Application of Polysiloxane to The Passivation of Semiconductor Devices," *Thin Solid Films*, vol. 33, pp. 35–41, 1976.

[16] Nowak, R., Schultz, F. A., Umana, M., Abruna, H., and Murray, R. W., "Chemically Modified Electrodes: Part XIV. Attachment of Reagents to Oxide-Free Glassy Carbon Surfaces. Electroactive RF Polymer Films on Carbon and Platinum Electrodes," *J. Electroanal. Chem.*, vol. 94, pp. 219–225, 1978.

[17] Daum, P., Lenhard, J. R., Rolison, D., and Murray, R. W., "Diffusional Charge Transport Through Ultrathin Films of Radiofrequency Plasma Polymerized Vinylferrocene at Low Temperature," *J. Am. Chem. Soc.*, vol. 102, pp. 4649–4653, 1980.

[18] Nowak, R. J., Schultz, F. A., Umana, M., Lam, R., and Murray, R. W., "Chemically Modified Electrodes. Radiofrequency Plasma Polymerization of Vinylferrocene on Glassy Carbon and Platinum Electrodes," *Anal. Chem.*, vol. 52, pp. 315–321, 1980.

[19] Daum P. and Murray, R. W. "Chemically Modified Electrodes: Part XXII. Solvent Effects on the Electrochemistry of Thin Films of Plasma Polymerized Vinylferrocene," *J. Electroanal. Chem.*, vol. 103, pp. 289–394, 1979.

[20] Shin, G. S., Kim, B. H., Hwang, Y. H., and Ko, Y. M., "Plasma Polymerization of 1,2- Diaminocyclohexane for Covalent Bonding of Bone Morphogenic Protein-2 on Titanium Surface," *J. Nanosci. Nanotechnol.*, vol. 15, pp. 5624–5627, 2015.

[21] Jatratkar, A. A., Yadav, J. B., Deshmukh, R. R., Barshilia, H. C., Puri, V., and Puri, R. K., "Glow Discharge Plasma Polymerized Nanostructured Polyaniline Thin Film Optical Waveguide," *Adv. Mater. Lett.*, vol. 8(2), pp. 180–184, 2017.

[22] Hirvonen and James K., "Ion Beam Assisted Thin Film Deposition," *Mater. Sci. Rep.*, vol. 6 (6), pp. 215–274, 1991.

[23] Frank F. S., "Developments in Plasma-Polymerized Organic Thin Films with Novel Mechanical, Electrical, and Optical Properties," *J. M. S.-rev.*, *Macromol. Chem. Phys.*, vol. 364, pp. 795–826, 1996.

[24] Kamal, M. M., and Bhuiyan, A. H., "Thickness Dependent Direct Current Electrical Conduction in Plasma Polymerized Pyrrole Monolayer Thin Films," *Adv. Mat. Res.*, vol. 741, pp. 59–64, 2013.

[25] Afroze, T., and Bhuiyan, A. H., "Effect of Heat Treatment on The Structural and Optical Characteristics of Plasma Deposited 2-(Diethylamino) Ethyl Methacrylate Thin Films by A Capacitively Coupled Glow Discharge Plasma System," *Phys. Scr.* vol. 88, pp. 045502, 2013.

[26] Rahman, M. J., and Bhuiyan, A. H., "Structural and Optical Properties of Plasma Polymerized o-Methoxyaniline Thin films," *Thin Solid Films*, vol. 534, pp. 132–136, 2013.

[27] Abbasi-Firouzjah M., and Shokri, B., "Deposition of High Transparent and Hard Optical Coating by Tetraethylorthosilicate Plasma Polymerization," *Thin Solid Films*, vol. 698, pp. 137857, 2020.

[28] Majumder, S., and Bhuiyan, A. H., "Direct Optical Transition in Plasma Polymerized Vinylene Carbonate Thin Films," *Indian J. Phys.*, vol. 85, pp. 1287–1297, 2011.

[29] Majumder, S. and Bhuiyan, A. H., "DC Conduction Mechanism in Plasma Polymerized Vinylene Carbonate Thin Films Prepared by Glow Discharge Technique," *Polym. Sci. Ser. A*, vol. 53, pp. 85–91, 2011.

[30] Sarker, R. B. and Bhuiyan, A. H., "Electrical Conduction Mechanism in Plasma Polymerized 1-Benzyl-2-Methylimidazole Thin Films Under Static Electric Field," *Thin Solid Films*, vol. 519, pp. 5912–5916, 2011.

[31] Manaa, C., Bouaziz, L., Lejeune, M., Kouki, F., Zellama, K., Benlahsen, M., Mejatty, M., and Bouchriha, H., "Detailed Investigation of Optoelectronic and Microstructural Properties of Plasma Polymerized Cyclohexane Thin Films: Dependence on the Radiofrequency Power," *J. Appl. Phys.*, vol. 117, pp. 215701–215708, 2015.

[32] Sanchis, M. R., Calvo, O., Fenollar, O., Garcia, D., and Balart, R., "Characterization of the Surface Changes and the Aging Effects of Low-Pressure Nitrogen Plasma Treatment in A Polyurethane Film," *Polym. Test.*, vol. 27, pp. 75–83, 2008.

[33] Momin, M. A., Hossain, K. S., and Bhuiyan, A. H., "Microstructural, Compositional, Topological and Optical Properties of Plasma Polymerized Cyclohexane Amorphous Thin Films," *J. Polym. Res.*, vol. 26, Article number: 83, 2019.

[34] Momin, M. A., and Bhuiyan, A. H., "Topological Properties and Direct Current Electrical Charge Transport Mechanism of Plasma Polymerized Cyclohexan Thin Films," *Thin Solid Films*, vol. 704, pp. 138014, 2020.

[35] Bayram, O., and Simsek, O., "Optical, chemical and dielectric properties of PPCIN films derived from essential oil using RF plasma polymerization," *Vacuum*, vol. 156, pp. 198–204, 2017.

[36] Golander, C. G., Rutland, M. W., Cho, D. L., Johansson, A., Ringblom, H., Jonsson, S., and Yasuda, H. K., "Structure and Surface Properties of Diaminocyclohexane Plasma Polymer Films," *J. App. Polym. Sci.*, vol. 49, pp. 39–51, 1993.

[37] Bae, I. S., Jung, C. K., Cho, S. J., Song, Y. H., and Boo, J. H., "A Comparative Study of Plasma Polymerized Organic Thin Films on Their Electrical and Optical Properties," *J. Alloys Compd.*, vol. 449, pp. 393–396, 2008.

[38] Shin, G. S, Kim, B. H., Hwang, Y. H., and Ko, Y. M., "Plasma Polymerization of 1,2-Diaminocyclohexane for Covalent Bonding of Bone Morphogenic Protein-2 on Titanium Surface," *J. Nanosci. Nanotechnol.*, vol. 15, pp. 5624–5627, 2015.

[39] Dinesh, P. R., Thanu, Srinadhu, E. S., Zhao, M., Nikhil, V. D., and Keswani, M., "*Developments in Surface Contamination and Cleaning: Applications of Cleaning Techniques,*" Chapter 8, pp. 289–353, 2019.

[40] Chen, F. F., "*Plasma Physics and Controlled Fusion,*" 2nd ed., Springer, New York, 2006.

[41] Dendy, R. O., "*Plasma Physics: An Introductory Course,*" Cambridge University Press, Cambridge, 1993.

[42] Lieberman, M. A., and Lichtenberg, A. J., "*Principles of Plasma Discharges and Materials Processing,*" John Wiley and Son's, New York, 1994.

[43] Yan, D., Sherman, J. H., and Keidar, M., "*Cold Atmospheric Plasma, A Novel Promising Anticancer Treatment Modality,*" Oncotarget, vol. 8, pp. 15977–15995 2016.

[44] Lee, H. J., Shon, C. H., Kim, Y. S., Kim, S., Kim, G. C., and Kong, M. G., "Degradation of Adhesion Molecules of G361 Melanoma Cells by a Non-Thermal Atmospheric Pressure Micro Plasma," *New J. Phys.*, vol. 11, pp. 115026, 2009.

[45] Takahashi, Y., Iijima, M., Inagawa, K., and Ito, "Synthesis of aromatic polyimide film by vacuum deposition polymerization," *J. Vac. Sci. Teclmol. A*, vol. 5, pp. 2253–2256, 1987.

[46] Kagami, Y., Yamauchi, T., and Osada, Y. "Preparation, Structure, and Electric Properties of Plasma-Polymerized Titanium Containing Organic Thin Films," *J. Appl. Phys.*, vol. 68, pp. 610–616, 1990.

[47] Morita, S., and Hattori, S., "*Applications of Plasma Polymers in Plasma Deposition, Treatment, and Etching of Polymers,*" (R. d'Agostino, Ed.), Academic Press, San Diego, CA, 1990.

[48] Hollahan, R., and Bell (Eds.), A. T., "*Techniques and Applications of Plasma Chemistry,*" Wiley, New York, 1974.

[49] Shen. M., and Bell, A. T., "*A Review of Recent Advances in Plasma Polymerization,*" Plasma Polymerization, American Chemical Society, Washington, D.C., 1979.

[50] Gombotz, W., and Hoffman, A., *J. Appl. Polym. Sci., Appl. Polym. Symp.*, vol. 2, pp. 285, 1988.

[51] Gombotz, W. R., Guanghui, W., and Hoffman, A. S., "Immobilization of Poly (Ethylene Oxide) on Poly (Ethylene Terephthalate) using a Plasma Polymerization Process," *J. Appl. Polym. Sci.*, vol. 37, pp. 91–107, 1989.

[52] Yasuda, H., and Hirotsu, T., "Critical Evaluation of Conditions of Plasma Polymerization," *J. Polym. Sci., Polym. Chem. Ed.*, vol.16, pp. 313–317, 1978.

[53] Yasuda, H., and Lamaze, C. E., "Polymerization in an electrode less glow discharge. III. Organic compounds without olefinic double bond," *J. Appl. Polym. Sci.*, vol. 17, pp. 1533–1544, 1973.

[54] Grill, A., "*Cold Plasma in Materials Fabrication: From Fundamentals to Applications,*" IEEE Press, New York, 1994.

[55] Bogaerts, A., Wilken, L., Hoffmann, V., Gijbels, R. and Wetzig, K., "Comparison of Modeling Calculations with Experimental Result for Rf Glow Discharge Optical Emission Spectroscopy," *Spectrochimi. Acta. Part B At. Spectrosc.*, vol. 57, pp.109–119, 2002.

[56] Mahan, J. E., "*Physical Vapor Deposition of Thin Films,*" John Wiley & Sons: New York, 2000.

[57] Simmons, J. G., "Poole-Frenkel Effect and Schottky Effect in MetalInsulator-Metal Systems," *Phys. Rev.*, vol. 115, pp. 657–660, 1967.

[58] Silverstein, M. S., and Visoy, F. I., "Plasma Polymerized Thiophene: Molecular Structure and Electrical Properties," *Polymer*, vol. 43, pp.11–20, 2002.

[59] Tolansky, "*Multiple Beam Interferometry,*" Oxford University Press, 1948.

[60] Mantravadi, M. V., "*Newton, Fizeau and Haidinger interferometers,*" Optical shop testing, New York: John Wiley & sons, Inc., pp. 19–36, 1992.

[61] John, D. W., "*Measurement of Film Thickness,*" McGraw-Hill, New York, 1967.

[62] Lamb, D. R., "*Electrical Conduction Mechanisms in Thin Insulating Films,*" Methuen and Co. Ltd., London, 1967.

[63] Banu, N., Bhuiyan, A. H., and Hossain, K. S., "Characterization of Structural and Optical Properties of Plasma Polymerized Diethanolamine Thin Films," *Adv. Polym. Technol.*, vol. 37, pp. 3084–3094, 2018.

[64] Nasrin, R., Rahman, M. J., Jamil, A. T. M. K., Hossain, K. S., and Bhuiyan, A. H., "Thickness Dependent Structural and Surface Properties of Plasma Polymerized N-Benzylaniline Thin Films," *Appl. Phys. A*, vol. 127, pp. 240, 2021.

[65] Horvath, R., Dregelyi-Kiss, A., and Matyasi, G., "The Examination of Surface Roughness Parameters in The Fine Turning of Hypereutectic Aluminium Alloys," *U.P.B. Sci. Bull., Ser. D*, vol. 77, pp. 205–216, 2015.

[66] Ba, E. C. T., Dumont, M. R., Martins, P. S., Drumond, R. M., Martins da Cruz, M. P., and Vieira, V. F., "Investigation of the Effects of Skewness R_{sk} and Kurtosis R_{ku} on Tribological Behavior in a Pin on-Disc Test of Surfaces Machined by Conventional Milling and Turning Processes," *Mat. Res.*; vol. 24(2), e20200435, 2021.

[67] Banwell, C. N., and Mc Cash, E. M., "*Fundamentals of Molecular Spectroscopy,*" McGraw-Hill, London, 1994.

[68] Silverstein, R. M., and Bassler, G. C., "*Spectroscopic Identification of Organic Compounds,*" John Wiley & Sons, New York, 1981.

[69] Golender, C. G., Rutland, M. W., and Cho, D. L., Johansson, A., Ringblom, H., Johansson, S., and Yasuda, H. K., "Structure and Surface Properties of Diaminocyclohexane Plasma Polymer Films," *J. Appl. Polym. Sci.*, vol. 49, pp. 39–51, 1993.

[70] Choukourov, A., Biederman, H., Kholodkov, I., Slavinska, D., Trchova, M., and Hollander, A., "Properties of Amine-Containing Coatings Prepared by Plasma Polymerization," *J. Appl. Polym. Sci.*, vol. 92, pp. 979–990, 2004.

[71] Yang, J., Lee, S., Park, H., and Jung, D., "Characterization of Low Dielectric Constant Plasma Polymer Films Deposited by Plasma-Enhanced Chemical Vapor Deposition Using Decamethylcyclopentasiloxane and Cyclohexane as the Precursors," *J. Vac. Sci. Technol. A*, vol. 24, pp. 165–169, 2006.

[72] Majumder, S., and Bhuiyan, A. H., "Effect of Heat Treatment on the Optical Properties of Plasma-Polymerized Vinylene Carbonate Thin Films," *Adv. Polym. Sci.*, vol. 34, pp. 21468(1–8), 2015.

[73] Kabir, H., Rahman, M. M., Roy, T. S., and Bhuiyan, A. H., "Structural and Optical Properties of Plasma Polymerized Pyromucic Aldehyde Thin Films," *Int. J. Mech. Mechatron. Eng.*, vol. 12, pp. 30–34, 2012.

[74] Chowdhury, F. U. Z., and Bhuiyan, A. H., "An Investigation of the Optical Properties of Plasma Polymerized Diphenyl Thin Films," *Thin Solid Films*, vol. 360, pp. 69–74, 2000.

[75] John, R. K., and Kumar, D. K., "Structural, Electrical and Optical Studies of Plasma Polymerized and Iodine Doped Polypyrrole," *J. Appl. Polym. Sci.*, vol. 83, pp. 1856 –1859, 2002.

[76] Bhattacharyya, S., Laha, A., and Krupanidhi, S. B., "Analysis of Leakage Current Conduction Phenomenon in Thin $SrBl_2Ta_2O_9$ Films Grown by Excimer Laser Ablation," *J. Appl. Phys.*, vol.91, pp. 4543– 4548, 2002.

[77] Pankove, J. I., "*Optical Processes in Semiconductors,*" Dover Publications Inc., New York, 1975.

[78] Eloy, J. F., "*Power Lasers,*" National School of Physics, Grenoble, France, John Wiley and Sons, 1984.

[79] Anderson, L. J., and Jacob, M. V., "Electrical Characterisations of Plasma Polyermised Linalyl Acetate," *Mater. Sci. Eng. B*, vol. 177, pp. 311– 315, 2012.

[80] Dakhel, A. A., "Mechanisms of DC-Current Transfer in Tris (Acetylacetonato) Iron (III) Films," *J. Non-Cryst. Solid.*, vol. 353, pp. 1529–1533, 2007.

[81] Matin, R., and Bhuniyan, A. H., "Electrical Transport Mechanism in Plasma Polymerized 2, 6, Diethylaniline Thin Films," *Thin Solid Films*, vol. 519, pp. 3462– 3467, 2011.

[82] Anderson, L. J., and Jacob, M. V., "Electrical Characterisations of Plasma Polyermised Linalyl Acetate," *Mater. Sci. Eng. B*, vol. 177, pp. 311–315, 2012.

[83] Gould, R. D., "The interpretation of space-charge-limited currents in semiconductors and insulators," *J. Appl. Phys.*, vol. 53, pp. 3353–3355, 1982.

[84] Ahmad, J., Bazaka, K., and Jacob, M. V., "Optical and Surface Characterization of Radio Frequency Plasma Polymerized 1-Isopropyl-4-Methyl-1,4-Cyclohexadiene Thin Films," *Electronics*, vol. 3, pp. 266–281, 2014.

[85] Kabir, H., Nasrin R., Rahman, M. M., and Bhuiyan, A. H., "Heat Treatment Effect on the Structural, Morphological, and Optical Properties of Plasma Polymerized Furan-2-Carbaldehyde Thin Films," *Results Phys.*, vol. 16, pp. 103014, 2020.

[86] Nasrin, R., Hossain, K. S., and Bhuiyan, A. H., "Morphological, Elemental, and Optical Characterization of Plasma Polymerized n-butyl Methacrylate Thin Films," *Appl. Phys. A*, vol. 124, pp. 391, 2018.